12

Optical Wave Turbulence in Fibers

Antonio Picozzi,[1] Josselin Garnier,[2] Gang Xu,[1] and Guy Millot[1]

[1] Laboratoire Interdisciplinaire CARNOT de Bourgogne, UMR 6303 CNRS-Université de Bourgogne - Franche-Comté, Dijon, France
[2] Centre de Mathématiques Appliquées, Ecole Polytechnique, Palaiseau, France

12.1 Introduction

The coherence properties of partially incoherent optical waves propagating in nonlinear media have been studied since the advent of nonlinear optics in the 1960s, because of the natural poor degree of coherence of laser sources available at that time. However, it is only recently that the dynamics of incoherent nonlinear optical waves received a renewed interest. The main motive for this renewal of interest is essentially due to the first experimental demonstration of incoherent solitons in photorefractive crystals [1,2]. The formation of an incoherent soliton results from the *spatial self-trapping* of incoherent light that propagates in a highly noninstantaneous response nonlinear medium [3,4]. This effect is possible because of the noninstantaneous photorefractive nonlinearity that averages the field fluctuations provided that its response time, τ_R, is much longer than the correlation time t_c that characterizes the incoherent beam fluctuations, i.e., $t_c \ll \tau_R$. The remarkable simplicity of experiments realized in photorefractive crystals has led to a fruitful investigation of the dynamics of incoherent nonlinear waves. Different theoretical approaches have been also developed to describe these experiments [5–8], which have been subsequently shown to be formally equivalent to each others [9,10].

In this way, the field of incoherent optical solitons has become a blooming area of research, as illustrated by several important achievements, e.g., the existence of incoherent dark solitons [11,12], the modulational instability of incoherent waves [13,14], incoherent solitons in periodic lattices [15,16], in resonant interactions [17,18], in liquid crystals [19], in nonlocal nonlinear media [20–22], or spectral incoherent solitons in optical fibers [23,24]. Nowadays, statistical nonlinear optics constitutes a growing field of research covering various topics of modern optics, e.g., supercontinuum generation [25], filamentation [26], random lasers [27], or extreme rogue wave events emerging from optical turbulence [28–32].

From a broader perspective, statistical nonlinear optics is fundamentally related to fully developed turbulence [33, 34], a subject which still constitutes one of the most challenging problems of theoretical physics [35,36]. In its broad sense, the kinetic wave

Shaping Light in Nonlinear Optical Fibers, First Edition. Edited by Sonia Boscolo and Christophe Finot.

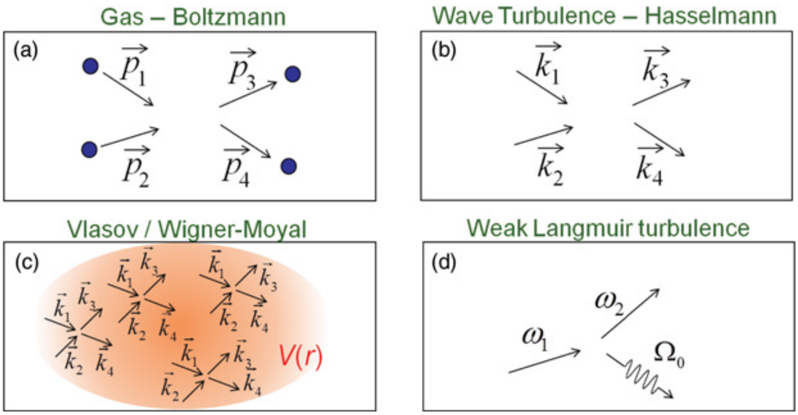

Figure 12.1 Analogy between a system of classical particles and the propagation of an incoherent optical wave in a Kerr medium. (a) As described by the kinetic gas theory, collisions between particles are responsible for an irreversible evolution of the gas towards thermodynamic equilibrium. (b) In complete analogy, the WT kinetic equation and the underlying four-wave mixing describe an irreversible evolution of the incoherent optical wave toward the thermodynamic Rayleigh-Jeans equilibrium state. (c) When the incoherent optical wave exhibits an inhomogeneous statistics, the quasi-particles feel the presence of an effective self-consistent potential, $V(r)$, which prevents them from relaxing to thermal equilibrium: The dynamics is described by a Vlasov-like kinetic equation. (d) In the presence of a noninstantaneous Raman-like nonlinearity, the causality condition inherent to the response function changes the physical picture, and the dynamics of the incoherent wave can be described by the weak Langmuir turbulence formalism.

theory provides a nonequilibrium thermodynamic description of developed turbulence. We schematically report in Figure 12.1 (a) qualitative and intuitive physical insight into the analogy which underlies the kinetic wave approach and the kinetic theory relevant to gas systems. We may note that the wave turbulence theory occupies a rather special place on the road-map of modern science, at the interface between applied mathematics, fluid dynamics, statistical physics and engineering. It has potential applications and implications in a diverse range of subjects including oceanography, plasma physics and condensed matter physics. The review article [37] was aimed at showing that the kinetic wave theory appears as the appropriate theoretical framework to formulate statistical nonlinear optics. In this chapter we illustrate the applicability of the kinetic wave theory to the specific example of optical fiber systems by considering three fundamentally different formalisms.

1. ***Wave turbulence formalism:*** Consider the nonlinear propagation of a partially coherent optical wave characterized by fluctuations that are statistically homogeneous in time (or in space). By complete analogy with a system of classical particles, the incoherent optical field evolves, owing to nonlinearity, towards a thermodynamic equilibrium state, as schematically illustrated in Figure 12.1 (a) and (b). A detailed theoretical description of the process of dynamical thermalization constitutes a difficult problem. However, a considerable simplification occurs when the dynamics is essentially dominated by linear dispersive effects, so that a weakly nonlinear description of the field becomes possible [33, 35, 36]. The weak- (or wave-)turbulence (WT) theory has been the subject of a lot of investigations in the context of plasma physics,

in which it is often referred to the so-called "random phase-approximation" approach [33, 38, 39]. This approach may be considered a convenient way of interpreting the results of the more rigorous technique based on a multi-scale expansion of the cumulants of the nonlinear field, as originally formulated in [40,41], and recently reviewed in [42]. The so-called "random phase approximation" may be considered justified when phase information becomes irrelevant to the wave interaction due to the strong tendency of the waves to decohere. The random phases can thus be averaged out to obtain a weak turbulence description of the incoherent wave interaction, which is formally based on irreversible kinetic equations [33]. The result is that, in spite of the formal reversibility of the equation governing wave propagation, the kinetic equation describes an irreversible evolution of the field to thermodynamic equilibrium. This equilibrium state refers to the fundamental Rayleigh-Jeans spectrum, whose tails are characterized by an equipartition of energy among the Fourier modes. The mathematical statement of such irreversible process relies on the H-theorem of entropy growth, whose origin is analogous to the Boltzmann's H-theorem relevant for gas kinetics.

Note that, besides this *nonequilibrium* kinetic approach, the equilibrium properties of a random nonlinear wave may be studied on the basis of *equilibrium* statistical mechanics by computing appropriate partition function [43–45]. In this way, the statistical properties of incoherent fields in random lasers have been analyzed by applying methods inherited from spun-glass theory [46]. In Section 12.2.1 we will review different processes of optical wave thermalization on the basis of the WT theory, while in Section 12.2.2 some mechanisms responsible for its inhibition will be discussed. In particular, we will see how the phenomenon of supercontinuum generation can be interpreted, under certain conditions, as a consequence of the natural thermalization of the optical field toward the thermodynamic equilibrium state. On the other hand, when a wave system is driven away from equilibrium by an external source, it no longer relaxes toward the Rayleigh-Jeans equilibrium distribution. A typical physical example of forced system can be the excitation of hydrodynamic surface waves by the wind. We will review in Section 12.2.3 recent important efforts aimed at providing a description of the turbulent dynamics of active and passive fiber cavities by means of a nonequilibrium kinetic formulation based on the wave turbulence equation.

2. ***Weak Langmuir turbulence formulation:*** When the incoherent wave propagates in a noninstantaneous Raman-like nonlinear medium, the dynamics turn out to be strongly affected by the causality property inherent to the nonlinear response function (see Figure 12.1). The kinetic wave theory reveals in this case that the appropriate description is provided by a formalism analogous to that used to describe weak Langmuir turbulence in plasmas [23,47]. A major prediction of the theory is the existence of spectral incoherent solitons [23, 24, 48]. This incoherent soliton is of a fundamental different nature from the incoherent solitons discussed here above. In particular, it does not exhibit a confinement in the spatiotemporal domain, but exclusively in the frequency domain. In Section 12.3, we will review the properties of these stable nonequilibrium incoherent states, as well as those associated to the formation of a novel form of spectral incoherent shock singularities [49].
3. ***Vlasov formalism:*** When the nonlinear material is characterized by a highly-noninstantaneous response (temporal nonlocality), the dynamics of the incoherent

wave turn out to be essentially governed by an effective nonlinear potential $V(r)$. This potential is self-consistent in the sense that it depends itself on the averaged intensity distribution of the random field, as schematically illustrated in Figure 12.1 (c). Actually, the mechanism underlying the formation of an incoherent localized soliton state finds its origin in the existence of such self-consistent potential, which is responsible for the self-trapping of the incoherent optical wave. In Section 12.4, we will review recent works in which the phenomena of incoherent modulational instability and incoherent localized temporal structures have been described in the framework of a Vlasov formalism. We note that such a Vlasov formalism differs from the traditional Vlasov equation considered for the study of incoherent modulational instability and incoherent solitons in plasmas [50, 51], hydrodynamics [52] and optics [8, 53–55]. The structure of this Vlasov equation is in fact analogous to that recently used to describe systems of particles with long-range interactions [56]. For this reason we will term this equation "long-range Vlasov" equation. It is important to underline that the long-range nature of a highly nonlocal nonlinear response prevents the wave system from reaching thermal equilibrium [22]. This fact can be interpreted intuitively in analogy with gravitational long-range systems and the Vlasov-like description of the dynamics of galaxies in the universe [56].

12.2 Wave Turbulence Kinetic Equation

In this section we illustrate the WT formalism by considering the process of optical wave thermalization through SC generation, as well as different mechanisms responsible for the inhibition of thermalization. We also review recent important efforts aimed at developing an appropriate kinetic description of the turbulent dynamics in optical cavities.

12.2.1 Supercontinuum Generation

The phenomenon of SC generation is characterized by a dramatic spectral broadening of the optical field during its propagation. This process has been extensively studied and different regimes have been identified, which essentially depend on whether the highly nonlinear photonic crystal fiber (PCF) is pumped in the normal or anomalous dispersion regimes, or with short (subpicosecond) or long (picosecond, nanosecond, and quasi-CW) pump pulses [25, 57].

As a rather general rule, the process of spectral broadening inherent to SC generation is interpreted through the analysis of the following main nonlinear effects: the four-wave mixing effect, the soliton fission, the Raman self-frequency shift and the generation of dispersive waves [57]. Due to such a multitude of nonlinear effects involved in the process, a complete and satisfactory theoretical description of SC generation is still lacking. However, there is a growing interest in developing new theoretical tools aimed at describing SC generation in more details. Besides the theories describing the interaction between individual soliton pulses and dispersive waves [58], we can quote the effective three-wave mixing theory and the underlying first-Born approximation successfully applied to describe femtosecond SC generation in different configurations [59,60]. We also mention recent works aimed at providing a complete characterization of the

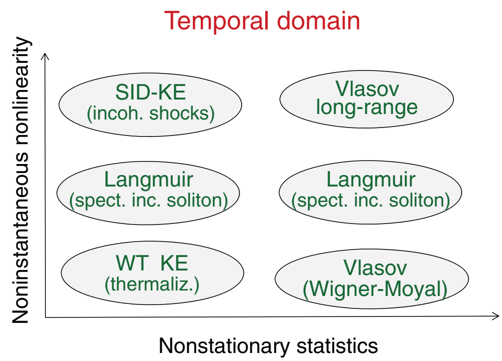

Figure 12.2 Schematic illustration of the validity of the fundamental kinetic equations. When the incoherent wave is characterized by fluctuations that are statistically stationary in time, the relevant kinetic description is provided by the WT kinetic equation. If the incoherent wave exhibits a nonstationary statistics, the relevant description is provided by the Vlasov formalism. If the response time of the nonlinearity can no longer be ignored, then the dynamics are ruled by the weak Langmuir turbulence formalism. If the random wave exhibits a non-stationary statistics in the presence of a highly noninstantaneous response, then the dynamics are governed by a long-range Vlasov formalism.

coherence properties of SC light by using second-order coherence theory of nonstationary light [61–63].

Incoherent Turbulent Regime of SC Generation The general physical picture of SC generation in PCFs can be summarized as follows. When the PCF is pumped with long pulses in the anomalous dispersion regime, MI is known to lead to the generation of a train of soliton-like pulses, which in turn lead to the emission of Cherenkov radiation in the form of spectrally shifted dispersive waves. These optical solitons are known to exhibit a self-frequency shift toward longer wavelengths as a result of the Raman effect. One encounters the same picture if the PCF is characterized by two zero dispersion wavelengths. In this case the Raman frequency shift of the solitons is eventually arrested in the vicinity of the second zero dispersion wavelengths. The SC spectrum then is essentially bounded by the corresponding dispersive waves [25, 58, 64–66]. The important aspect to underline here is that in all these regimes the existence of coherent soliton structures plays a fundamental role in the process of SC generation.

This physical picture of SC generation changes in a significant way when one considers the regime in which long and intense pump pulses are injected into the PCF. Indeed, in this highly nonlinear regime, the spectral broadening process is essentially dominated by the combined effects of the Kerr nonlinearity and higher-order dispersion, i.e., by four-wave mixing processes [67]. In this regime the optical field exhibits rapid and random temporal fluctuations, which prevent the formation of robust and persistent coherent soliton structures. It turns out that the optical field exhibits an incoherent turbulent dynamics, in which coherent soliton structures do not play any significant role. In the following we shall term this regime the “incoherent regime of SC generation” [68].

Wave Turbulence Approach to SC Generation In these last few years a nonequilibrium thermodynamic interpretation of this incoherent regime of SC generation has been formulated [24, 48, 68–70] on the basis of the WT theory. This WT description can be introduced through the analysis of the numerical simulation in Figure 12.3 (a). It reports a typical evolution of the spectrum of the optical field in the incoherent regime of SC generation. It is obtained by integrating numerically the generalized nonlinear Schrödinger (NLS) equation (see Eq. (12.1)), with the dispersion curve reported in Figure 12.3 (b).

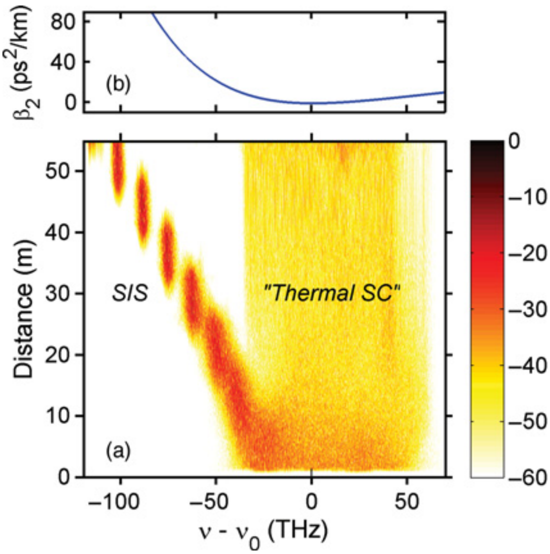

Figure 12.3 Incoherent turbulent regime of SC generation: (a) Numerical simulations of the generalized NLS Eq. (12.1) reporting the spectral evolution as a function of propagation distance in a 50m long PCF, for an input CW power equal to 200W ($\gamma = 0.05\ \mathrm{W^{-1}m^{-1}}$). The corresponding dispersion curve of the PCF used in the simulations is illustrated in (b). The optical spectrum is characterized by two main features: (i) A broad central part governed by the four-wave mixing process that exhibits a process reminiscent of thermalization. (ii) A narrower low-frequency branch governed by the Raman effect that self-organizes into a continuous, and subsequently a discrete, spectral incoherent soliton (see Section 12.3).

The initial condition is a high-power (200 W) continuous wave whose carrier frequency $\nu_0 = 283$ THz ($\lambda_0 = 1060$ nm) lies in the anomalous dispersion regime and thus leads to the development of the modulational instability process.

We note in Figure 12.3 (a) that the spectrum of the field essentially splits into two components during the propagation:

(i) On the one hand, one notices a broad central part whose evolution is essentially governed by the dispersion effects and the Kerr nonlinearity. These effects are inherently conservative effects and lead to a process of wave thermalization through SC generation, a feature that has been discussed in [68–70] using the WT theory. Accordingly, the saturation of SC spectral broadening can be ascribed to the natural tendency of the optical field to reach an equilibrium state. Note, however, that, as will be discussed below, the phenomenon of wave thermalization through SC generation is not achieved in a complete fashion, in the sense that the tails of the numerical spectra exhibit some discrepancy with the corresponding expected tails of the Rayleigh-Jeans distribution. While this discrepancy can be simply ascribed to a limited propagation length in the PCF, another possible physical origin of such discrepancy will be discussed in Section 12.2.2.1. This WT approach also reveals the existence of an unexpected phase-matching process that can be interpreted on the basis of thermodynamic properties.

(ii) On the other hand, one notices in Figure 12.3 (a) that a low-frequency spectral branch moves away from the central part of the spectrum. This low-frequency branch is essentially governed by the dissipative Raman effect, whose noninstantaneous nonlinear nature is responsible for the generation of spectral incoherent solitons, a feature that will be discussed in Section 12.3.

12.2.1.1 Generalized NLS Equation

The generalized NLS equation is known to provide an accurate description of the propagation of an optical field in a PCF [57,71],

$$i\frac{\partial\psi(z,t)}{\partial z} + \sum_{j\geq 2}^{m} \frac{i^j\beta_j}{j!}\frac{\partial^j\psi(z,t)}{\partial t^j} + \gamma\left(1 + i\tau_s\frac{\partial}{\partial t}\right)\psi(z,t) \times \int_{-\infty}^{+\infty} R(t')\,|\psi(z,t-t')|^2\,dt' = 0, \tag{12.1}$$

where we note that γ refers to the nonlinear coefficient and $R(t) = (1-f_R)\delta(t) + f_R h_R(t)$ to the usual nonlinear response function of silica fibers, which accounts for both the instantaneous Kerr effect and the non-instantaneous Raman response function $h_R(t)$ $[\tilde{\psi}(\omega,z) = (2\pi)^{-1/2}\int \psi(t,z)\,\exp(i\omega t)\,dt]$ [71]. The linear dispersion relation of Eq. (12.1) reads $k(\omega) = \sum_{j\geq 2}^{m} \frac{\beta_j\omega^j}{j!}$.

As discussed above through Figure 12.3 (a), wave thermalization is driven by the combined effects of dispersion and Kerr nonlinearity, which are inherently conservative effects. On the other hand, the Raman effect [$f_R \neq 0$ in Eq. (12.1)] is a dissipative effect and prevents the establishment of a thermodynamic equilibrium state (see Section 12.3). Note that this is consistent with the fact that the Raman effect breaks the Hamiltonian structure of Eq. (12.1). In this section we will thus ignore the dissipative Raman effect.

We report in Figure 12.4 (a) exactly the same numerical simulation as that reported in Figure 12.3 (a), except that we removed the Raman effect, $f_R = 0$ in Eq. (12.1). We also removed in this simulation the influence of the shock term ($\tau_s = 0$), whose influence has

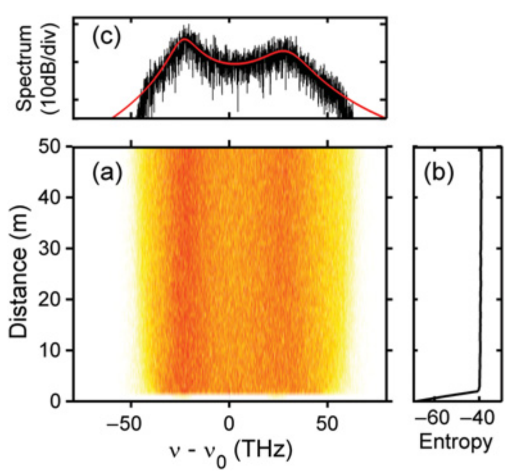

Figure 12.4 Optical wave thermalization through SC generation. (a) Same as in Figure 12.3 (a), except that the Raman effect and the shock term have been neglected, $f_R = \tau_s = 0$: this simulations thus refers to the numerical integration of the instantaneous NLS Eq. (12.2). (b) Optical wave thermalization is characterized by a process of entropy production, which saturates to a constant level once the equilibrium state is reached, as described by the H−theorem of entropy growth. (c) Comparison of the the thermodynamic Rayleigh-Jeans equilibrium spectrum $n^{eq}(\omega)$ (Eq. (12.5)) (continuous line), and the numerical spectrum corresponding to an averaging over the last 20m of propagation. A good agreement is obtained without adjustable parameters – note, however, a discrepancy in the tails of the spectrum (see the text for discussion).

been considered in [70]. Comparison of Figures 12.3 (a) and 12.4 (a) clearly shows that the essential role of the Raman effect is to lead to the generation of a spectral incoherent soliton in the low-frequency branch in the SC spectrum. Besides spectral incoherent solitons, a peculiar feature revealed by Figure 12.4 (a) is that the spectral broadening inherent to SC generation saturates during the propagation, a feature related to the thermalization of the optical field.

12.2.1.2 Wave Thermalization through Supercontinuum Generation

Neglecting the Raman effect and the shock term, the generalized NLS Eq. (12.1) reduces to

$$i\frac{\partial\psi}{\partial z} + \sum_{j\geqslant 2}^{m} \frac{i^j \beta_j}{j!}\frac{\partial^j \psi}{\partial t^j} + \gamma|\psi|^2\psi = 0. \tag{12.2}$$

We recall that, if only the second-order dispersion effect is retained ($m = 2$), Eq. (12.2) recovers the completely integrable 1D-NLS equation. The corresponding infinite number of conserved quantities prevents the thermalization of the wave toward thermodynamic equilibrium, though the system still exhibits a relaxation toward an equilibrium state of a different nature [72, 73]. This aspect will be discussed in Section 12.2.2.

If one includes the influence of third-order dispersion ($m = 3$), the system exhibits a process of anomalous thermalization [74, 75], which is characterized by an irreversible evolution toward an equilibrium state of a fundamental different nature than the thermodynamic equilibrium state. This previous work [75] can be important to study the evolution of an incoherent wave in a PCF characterized by a single zero dispersion wavelength, and will be discussed in Section 12.2.2.

If one includes dispersion effects up to the fourth-order ($m = 4$), the simulations reveal the existence of a phenomenon of "truncated thermalization": The incoherent wave exhibits an irreversible evolution toward the Rayleigh-Jeans thermodynamic equilibrium state characterized by a compactly supported spectral shape. This aspect will be discussed in Section 12.2.2.

Thermodynamic Equilibrium Spectrum In the following we consider realistic dispersion curves of PCFs characterized by two zero dispersion wavelengths, whose accurate description requires a high-order Taylor expansion of the dispersion relation ($m > 4$ and even). Starting from the high-order dispersion NLS Eq. (12.2), one can derive the irreversible WT kinetic equation governing the evolution of the averaged spectrum of the field $n(z, \omega)$ $[\langle\tilde{\psi}(z, \omega_1)\tilde{\psi}^*(z, \omega_2)\rangle = n(z, \omega_1)\,\delta(\omega_1 - \omega_2)]$:

$$\partial_z n(z, \omega_1) = Coll[n], \tag{12.3}$$

with the collision term

$$Coll[n] = \iiint d\omega_2\, d\omega_3\, d\omega_4\; n(\omega_1)n(\omega_2)n(\omega_3)n(\omega_4) \\ \times W\left[n^{-1}(\omega_1) + n^{-1}(\omega_2) - n^{-1}(\omega_3) - n^{-1}(\omega_4)\right] \tag{12.4}$$

where "$n(\omega)$" stands for "$n(z, \omega)$" in Eq. (12.4). As usual in the WT kinetic equation, the phase-matching conditions of energy and momentum conservation are expressed by the presence of Dirac δ−functions in $W = \frac{\gamma^2}{\pi}\,\delta(\omega_1 + \omega_2 - \omega_3 - \omega_4)\,\delta[k(\omega_1) + k(\omega_2) - k(\omega_3) - k(\omega_4)]$, where $k(\omega)$ refers to the linear dispersion relation. Equation (12.3) conserves the power density $N/T_0 = \int n(z,\omega)\,d\omega$, the density of kinetic energy $E/T_0 = \int k(\omega)\,n(z,\omega)\,d\omega$ and the density of momentum $P/T_0 = \int \omega\,n(z,\omega)\,d\omega$, where T_0 refers to the considered numerical time window. It also exhibits a H-theorem of entropy growth, $\partial_z \mathcal{S} \geqslant 0$, where the nonequilibrium entropy reads $\mathcal{S}(z) = \int \log[n(z,\omega)]\,d\omega$. The Rayleigh-Jeans equilibrium distribution is obtained by maximizing the entropy under the constraints imposed by the conservation of the energy, momentum and power, which gives

$$n^{eq}(\omega) = \frac{T}{k(\omega) + \lambda\omega - \mu}, \tag{12.5}$$

where T and μ are by analogy with thermodynamics the temperature and the chemical potential of the incoherent wave at equilibrium. The three parameters (T,μ,λ) are calculated from the conserved quantities (E,N,P) by substituting the equilibrium spectrum Eq. (12.5) into the definitions of E, N and P. One thus obtains an algebraic system of three equations for three unknown parameters, which can be solved numerically. A unique triplet solution (T,μ,λ) for a given set (E,N,P) is usually obtained, a feature which is consistent with the fact that a "closed" (conservative and Hamiltonian) system should exhibit a unique thermodynamic equilibrium state.

The meaning of the parameter λ becomes apparent through the analysis of the group-velocity v_g of the optical field $[k'(\omega) \equiv \partial k/\partial\omega = 1/v_g(\omega)]$. Indeed, recalling the definition of an average, $\langle \mathcal{A} \rangle_{eq} = \int \mathcal{A}\,n^{eq}(\omega)\,d\omega / \int n^{eq}(\omega)\,d\omega$ and making use of the equilibrium spectrum Eq. (12.5), one readily obtains

$$< k'(\omega) >_{eq} = -\lambda. \tag{12.6}$$

According to relation (12.6), the parameter λ denotes the average of the inverse of the group-velocity of the optical field at equilibrium. We report in Figure 12.4 (c) the comparison of the theoretical prediction (12.5) with the results of the numerical simulations of the high-order NLS Eq. (12.2). A quantitative agreement is obtained between the simulations and the theory Eq. (12.5), without using adjustable parameters. The Rayleigh-Jeans spectrum is characterized by a double-peaked structure, which results from the presence of two zero dispersion wavelengths in the dispersion curve of the PCF. The relaxation toward thermal equilibrium is also corroborated by the saturation of the process of entropy production illustrated in Figure 12.4 (b). Note, however, that a notable discrepancy is visible in the tails of the spectrum in Figure 12.4 (c), as if the thermalization process were not achieved in a complete fashion. Actually, the simulations reveal that the tails of the spectrum exhibit a very slow process of spectral broadening, which apparently tends to evolve toward the expected Rayleigh-Jeans tails – though the required propagation length is extremely large. This aspect will be discussed in more detail in Section 12.2.2 in the particular case where the dispersion relation is truncated to the fourth-order ($m = 4$ in the dispersion relation). The good agreement between the theory and the simulations has been obtained in a variety of configurations, e.g., under cw or incoherent pumping, as discussed in detail in [69,70].

Thermodynamic Phase-Matching The thermodynamic equilibrium spectrum given in Eq. (12.5) is characterized by a double peak structure, which originates from the two zero dispersion wavelengths that characterize the PCF dispersion curve. It is important to underline, however, that the frequencies (ω_1, ω_2) of the two peaks of $n^{eq}(\omega)$ do not simply correspond to the minima of the dispersion relation, i.e. $k'(\omega_{1,2}) \neq 0$. To further analyze this aspect, let us write the thermodynamic equilibrium spectrum in the form $n^{eq}(\omega) = T/\mathcal{F}(\omega)$, with $\mathcal{F}(\omega) = k(\omega) + \lambda\omega - \mu$. The two frequencies (ω_1, ω_2) which maximize the equilibrium spectrum (12.5) satisfy $\mathcal{F}'(\omega_1) = \mathcal{F}'(\omega_2) = 0$, i.e., $k'(\omega_1) = k'(\omega_2) = -\lambda$. This observation reveals that the two frequencies (ω_1, ω_2) of the double peaked equilibrium spectrum (12.5) are selected in such a way that the corresponding group-velocities coincide with the average group-velocity of the optical wave,

$$v_g(\omega_1) = v_g(\omega_2) = 1/\langle k'(\omega)\rangle_{eq} = -1/\lambda. \tag{12.7}$$

It can be shown that there exists, in principle, a unique pair of frequencies (ω_1, ω_2) satisfying the conditions given by Eq. (12.7). In other terms, for a given thermodynamic equilibrium spectrum (12.5), there exists a *unique* pair of frequencies (ω_1, ω_2) that leads to a matched group-velocity of the double peaked spectrum [70]. In this sense, Eq. (12.7) can be regarded as a thermodynamic phase-matching condition.

The thermodynamic phase-matching given by Eq. (12.7) then imposes a matching of the group-velocities of the two spectral peaks of the SC spectrum. The fact that different wave-packets naturally tend to propagate with the same group-velocity was discussed in [76]. This can be interpreted by analogy with basic equilibrium thermodynamic properties, namely that an isolated system can only exhibit a uniform motion of translation (and rotation) as a whole, while any macroscopic internal motion is not possible at thermodynamic equilibrium [77]. In this way, it was shown that a velocity locking is required, in the sense that it prevents "a macroscopic internal motion in the wave system." We refer the interested reader to [37, 70] for more details on this aspect.

12.2.2 Breakdown of Thermalization

A fundamental assumption of statistical mechanics is that a closed system with many degrees of freedom ergodically samples all equal energy points in phase space. In order to analyze the limits of this assumption, Fermi, Pasta and Ulam (FPU) considered in the 1950s a one-dimensional chains of particles with anharmonic forces between them [78]. They argued that, owing to the nonlinear coupling, an initial state in which the energy is in the first few lowest modes would eventually relax to a state of thermal equilibrium where the energy is equidistributed among all modes on the average. However, they observed that, instead of leading to the thermalization of the system, the energy transfer process involves only a few modes and exhibits a reversible behavior, in the sense that after a sufficiently (long) time the system nearly goes back to its initial state. Fundamental mathematical and physical discoveries, like the Kolmogorov-Arnold-Moser theorem and the formulation of the soliton concept, have led to a better understanding of the Fermi-Pasta-Ulam problem, although it is still the subject of intense research activity, see e.g., [78–80].

We should note that, in spite of the large number of theoretical studies, experimental demonstrations of FPU recurrences have been reported in very few systems. In particular, the FPU recurrences associated with modulational instability of the NLS equation have been experimentally studied in deep water waves [81], and, more recently, in magnetic feedback rings [82] and optical wave systems [79,83–85]. By considering the one-dimensional NLS equation, we present in this section three different mechanisms that inhibit the process of optical wave thermalization toward the Rayleigh-Jeans distribution. Depending on whether the dispersion relation is truncated up to the second, third, or fourth-order, the wave system exhibits different types of relaxation processes. Provided that the interaction occurs in the weakly nonlinear regime, the WT theory provides an accurate description of such mechanisms of breakdown of thermalization.

12.2.2.1 Fourth-Order Dispersion: Truncated Thermalization

We consider here the 1D NLS equation in which the dispersion relation is truncated to the fourth-order. In this case, the WT theory reveals the existence of an irreversible evolution toward a Rayleigh-Jeans equilibrium state characterized by a compactly supported spectral shape [86]. This phenomenon of truncated thermalization may explain the physical origin of the abrupt SC spectral edges discussed above in Section 12.2.1.2. More generally, it can shed new light on the mechanisms underlying the formation of bounded spectra in SC generation [64–66, 87]. Besides its relevance in the context of SC generation, this phenomenon is also important from a fundamental point of view. Indeed, it unveils the existence of a genuine frequency cut-off that arises in a system of classical waves described by the generalized NLS equation, a feature of importance considering the well-known ultraviolet catastrophe of ensemble of classical waves [37].

The starting point is the NLS Eq. (12.2) accounting for third- and fourth-orders dispersion effects, as well as the corresponding WT kinetic Eq. (12.3). The kinetic theory reported in [86] reveals that the process of thermalization to the Rayleigh-Jeans spectrum (12.5) is not achieved in a complete way, but turns out to be truncated within a specific frequency interval defined by the bounds, $\omega \in [\omega_-, \omega_+]$, with

$$\omega_\pm = -\frac{\tilde{\alpha}}{4\tilde{\beta}\tau_0} \pm \frac{\sqrt{21}}{12\tilde{\beta}\tau_0}\sqrt{3\tilde{\alpha}^2 + 8\tilde{\beta}}, \tag{12.8}$$

where $\tilde{\alpha}$ and $\tilde{\beta}$ refer to the normalized third- and fourth-orders dispersion parameters, namely $\tilde{\alpha} = L_{nl}\beta_3/\left(6\tau_0^3\right)$, and $\tilde{\beta} = L_{nl}\beta_4/\left(24\tau_0^4\right)$, where $\tau_0 = \sqrt{\beta_2 L_{nl}/2}$ is the corresponding healing time, i.e., the characteristic time for which linear and nonlinear effects are of the same order of magnitude [37].

The confirmation of this process of truncated thermalization by the numerical simulations has not been a trivial task. This is due to the fact that in the usual configurations of SC generation discussed above, the cascade of MI side-bands generated by the cw pump in the early stage of propagation spreads beyond the frequency interval predicted by the theory. As already discussed, the MI process is inherently a coherent nonlinear phase-matching effect which is not described by the WT kinetic equation (Eqs. (12.3) and (12.4)). This explains why the numerical simulations reported above (or in [69,70]) did not evidence a precise signature of this phenomenon of truncated thermalization.

In order to analyze the theoretical predictions in more detail, one needs to decrease the injected pump power so as to maintain the (cascaded) MI side-bands within the frequency interval (12.8). Intensive numerical simulations of the NLS equation in this regime of reduced pump power have been performed in [86]. This study reveals that the nonlinear dynamics slows down in a dramatic way, so that the expected process

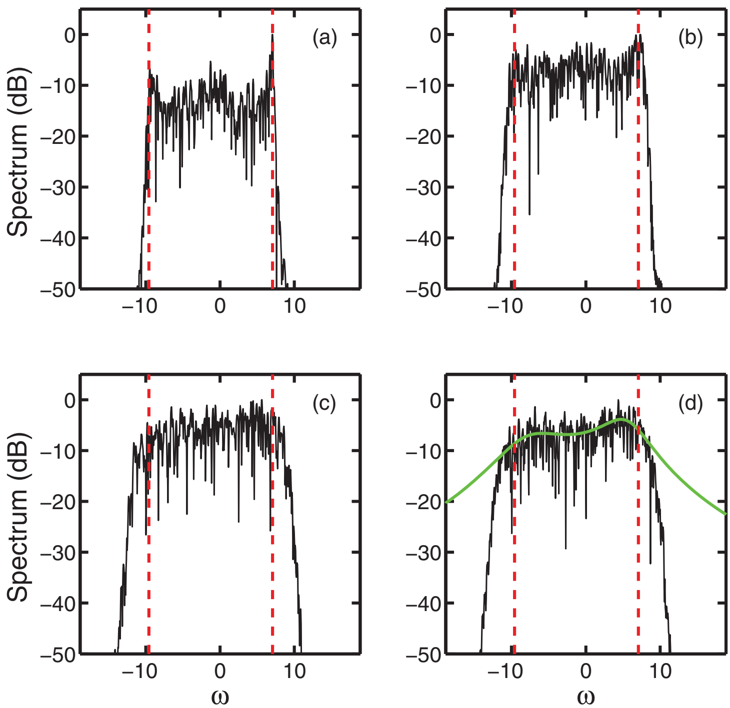

Figure 12.5 Truncated thermalization of incoherent waves: Spectra $|\tilde{\psi}|^2(\omega, z)$ obtained by solving the NLS Eq. (12.2) with solely third and fourth-order dispersion effects ($\tilde{\alpha} = 0.1$, $\tilde{\beta} = 0.02$): (a) $z = 200$, (b) $z = 10^4$, (c) $z = 5 \times 10^5$, (d) $z = 10^6$. After a long transient, the wave relaxes toward a truncated Rayleigh-Jeans distribution (Eq. (12.5), continuous line) (d). The dashed lines denote the frequencies $\omega_\pm$ in Eq. (12.8) – ω is here in units of τ_0^{-1}. *Source*: Barviau 2013 [86]. Reproduced with permission of American Physical Society.

of thermalization requires huge nonlinear propagation lengths. This results from the fact that the normalized parameters $\tilde{\alpha}$ and $\tilde{\beta}$ decrease as the pump power decreases, so that the NLSE approaches the integrable limit, which does not exhibit thermalization [73] (see Section 12.2.2.3). We report in Figure 12.5 the wave spectra at different propagation lengths obtained by solving the NLS equation with $\tilde{\alpha} = 0.1$ and $\tilde{\beta} = 0.02$. In the early stage of propagation, $z \sim 200$, the spectrum remains confined within the frequency interval $[\omega_-, \omega_+]$ predicted by the theory (Eq. (12.8)), although the spectrum exhibits a completely different spectral profile than the expected Rayleigh-Jeans distribution. As a matter of fact, the process of thermalization requires enormous propagation lengths, as illustrated in Figure 12.5 (d), which shows that the wave spectrum eventually relaxes toward a truncated Rayleigh-Jeans distribution. For more details on these numerical simulations, we refer the reader to [37].

12.2.2.2 Third-Order Dispersion: Anomalous Thermalization

Here we discuss another mechanism that inhibits the natural process of thermalization. We consider the 1D NLS equation by truncating the dispersion relation up to the third order. We will see that the incoherent wave exhibits an irreversible evolution toward an equilibrium state of a different nature than the conventional

Rayleigh-Jeans equilibrium state. The WT kinetic equation reveals that this effect of anomalous thermalization is due to the existence of a local invariant in frequency space J_ω, which originates in degenerate resonances of the system [74,75]. In contrast to conventional integral invariants that lead to a generalized Rayleigh-Jeans distribution, here, it is the local nature of the invariant J_ω that makes the new equilibrium states different from the usual Rayleigh-Jeans equilibrium states. We remark that local invariants and the associated process of anomalous thermalization have also been identified in the 1D vector NLS equation, a configuration in which optical fiber experiments have been also performed, see [74].

The starting point is the NLS Eq. (12.2) accounting for third-order dispersion effects, as well as the corresponding WT kinetic Eq. (12.3). A refined analysis of the WT kinetic equation reveals a remarkable property, namely the existence of a local invariant in frequency space:

$$J(\omega) = n(\omega, z) - n(q - \omega, z), \tag{12.9}$$

where $q = 2s\omega_*$, ω_* being the zero-dispersion angular frequency, and $s = \mathrm{sign}(\beta_2)$ [74,75]. This invariant is “local” in the sense that it is verified for each frequency ω individually, $\partial_z J(\omega) = 0$. It means that the subtraction of the spectrum by the reverse of itself translated by q, remains invariant during the whole evolution of the wave. The invariant (12.9) finds its origin in the following degenerate resonance of the phase-matching conditions: a pair of frequencies $(\omega, q - \omega)$ may resonate with any pair of frequencies $(\omega', q - \omega')$, because $k(\omega) + k(q - \omega) = sq^2/3$ does not depend on ω. Because of the existence of this local invariant, the incoherent wave relaxes toward an equilibrium state of fundamental different nature from the expected thermodynamic Rayleigh-Jeans spectrum:

$$n^{loc}(\omega) = \frac{J_\omega}{2} + \frac{1}{\lambda}\left(1 + \sqrt{1 + \left(\frac{\lambda J_\omega}{2}\right)^2}\right). \tag{12.10}$$

Here, the parameter λ is determined from the initial condition through the conservation of the power. We remark that the equilibrium distribution Eq. (12.10) vanishes exactly the collision term of the kinetic equation, i.e., it is a stationary solution. The equilibrium distribution is characterized by a remarkable property: it exhibits a constant spectral pedestal, $n^{loc}(\omega) \to 2/\lambda$ for $|\omega| \gg |\omega_*|$. We remark in this respect that in the tails of the spectrum ($|\omega| \gg |\omega_*|$), the invariant J_ω vanishes, so that a constant spectrum ($n_\omega = const$) turns out to be a stationary solution of the WT kinetic equation. The existence of the process of anomalous thermalization has been confirmed by the numerical simulations of both the NLS equation and the WT kinetic equation, as illustrated in Figure 12.6 in the color plate section. For more details on theoretical and numerical simulations of anomalous thermalization, we refer the reader to [37,75,88].

12.2.2.3 Second-Order Dispersion: Integrable Limit

In this section we consider the case where the dispersion relation of the NLS equation is truncated to the second-order, so that the equation recovers the completely integrable NLS equation which is known to admit genuine soliton solutions. During the past fifty years, the question of the interaction among solitons has been extensively studied

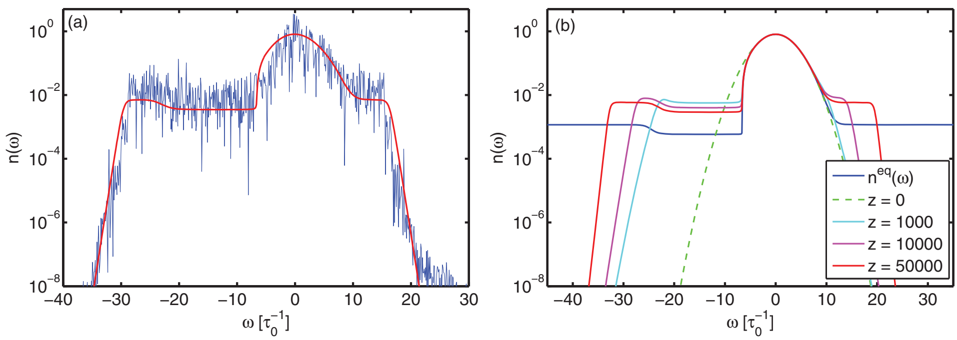

Figure 12.6 Anomalous thermalization of incoherent waves: (a) Spectral evolution obtained by integrating numerically the NLSE with third-order dispersion (blue) and the corresponding WT kinetic equation (red) at $z = 20000$ for $\tilde{\alpha} = 0.05$ (a). (b) Numerical simulations of the WT kinetic equation showing the spectral profile $n(z, \omega)$ at different propagation lengths z: a constant spectral pedestal emerges in the tails of the spectrum ($\tilde{\alpha} = 0.05$). The spectrum slowly relaxes toward the equilibrium state $n^{loc}(\omega)$ given by Eq. (12.10) (blue). *Source*: Michel 2011 [88]. For a color version of this figure please see color plate section.

by using the method of the inverse scattering transform (see, e.g., [89]). From a different perspective, the formation and the dynamics of shock-waves in the defocusing regime have been studied in different experimental circumstances (see, e.g., [90–92]). The evolution of a dense gas of uncorrelated NLS solitons has been also examined in [93], in which a general method to derive kinetic equations describing the evolution of the spectral distribution function of solitons has been proposed.

The non-integrability of the model equation is usually considered a prerequisite for the applicability of WT theory: Applying the conventional WT procedure to the integrable NLS equation, one finds that all collision terms in the kinetic equation vanish identically at any order [94]. Accordingly, the traditional WT procedure predicts that the spectrum of a weakly nonlinear wave does not evolve during the propagation. We note in this respect that accurate experiments have been performed in optical fibers since 2006 [95], which revealed that a significant evolution of the spectrum of the wave occurs beyond the weakly nonlinear regime of propagation. This issue was subsequently addressed in [72,73], in which a generalized WT kinetic equation was proposed by considering that the fourth-order moment of the field is not necessarily a stationary quantity. It is important to note that similar generalizations of the WT kinetic equation were originally developed in the context of hydrodynamic waves (see [96] for a review), and are still important when one considers the early stage of the evolution of the turbulent system, see, e.g., [97]. From a broader perspective, the study of wave turbulence in the framework of integrable, e.g., NLS, equations is an important field of research which is attracting a growing interest in relation, e.g., with the phenomenon of intermittency [98], or the formation of extreme rogue wave events [32, 99].

The starting point is the NLS Eq. (12.2) accounting solely for second-order dispersion. Since exact resonant interactions lead to a vanishing collision term in the conventional kinetic equation, the idea here is to derive a generalized kinetic equation by considering quasi-resonant four-wave interactions, i.e., interactions that do not verify the phase-matching condition, $\Delta k = k(\omega_1) + k(\omega_2) - k(\omega_3) - k(\omega_4) = 0$, where

$k(\omega) = \beta_2\omega^2/2$. In this way, one can derive a generalized form of the kinetic equation:

$$\partial_z n_{\omega_1}(z) = \frac{\gamma^2}{\pi^2} \int_0^z dz' \int\int\int Q[n(z')] \cos[\Delta k(z'-z)] \times \delta(\omega_1 + \omega_2 - \omega_3 - \omega_4)\, d\omega_2 d\omega_3 d\omega_4. \quad (12.11)$$

where $Q[n] = n_{\omega_1}(z)n_{\omega_3}(z)n_{\omega_4}(z) + n_{\omega_2}(z)n_{\omega_3}(z)n_{\omega_4}(z) - n_{\omega_1}(z)n_{\omega_2}(z)n_{\omega_3}(z) - n_{\omega_1}(z) n_{\omega_2}(z)n_{\omega_4}(z)$. Because of the presence of the cosine function, the collision term of this kinetic equation no longer vanishes, despite the degenerate phase-matching interaction. Actually, the evolution of the spectrum described by Eq. (12.11) is characterized by the rapid growth of spectral tails that exhibit damped oscillations, until the whole spectrum ultimately reaches a statistically stationary state. The kinetic equation provides an analytical expression of the damped oscillations, which is found in agreement with the numerical simulations of both the NLS and kinetic equations [73]. An interesting experiment aimed at observing this phenomenon of irreversible relaxation in the limit of the integrable NLS equation has been reported in [73], see Figure 12.7.

We conclude this paragraph by reminding that the applicability of the generalized WT kinetic equation to the description of the dynamics of the integrable NLS equation is constrained by the usual assumption of weakly nonlinear interaction. A rigorous mathematical treatment of the evolution of the incoherent wave beyond this weakly nonlinear regime would require the application of the inverse scattering machinery (see, e.g., [100,101]), a feature which is also of interest considering the recent Hanbury Brown and Twiss experiment [102,103].

12.2.3 Turbulence in Optical Cavities

The phenomenon of wave thermalization can be characterized by a self-organization process, in the sense that it is thermodynamically advantageous for the system to generate a large-scale coherent structure in order to reach the most disordered equilibrium state. A remarkable example of this counterintuitive phenomenon is provided by wave

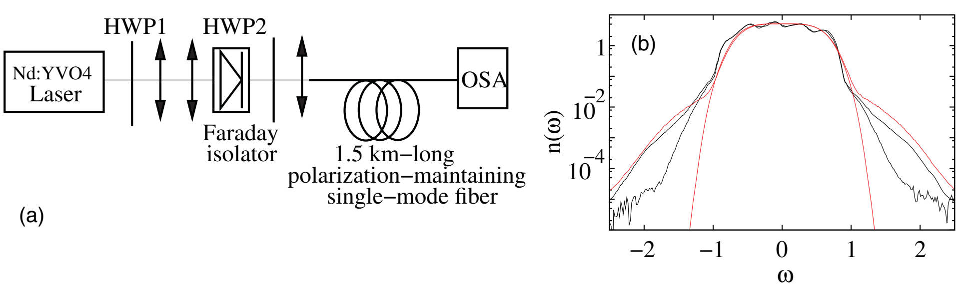

Figure 12.7 Irreversible relaxation process of the integrable NLS equation. (a) Shematic representation of the experimental setup. HWP: half-wave plate. OSA: optical spectrum analyzer. (b) Spectra recorded in experiments (black lines) and obtained from numerical simulations (red lines) of the integrable NLS equation. Note that numerical simulations of a reduced form of the kinetic Eq. (12.11) provide identical results (not represented here, see [73]). The narrow spectrum plotted in the black line is the spectrum of the Nd:YVO4 laser launched inside the polarization maintaining fiber. The wide spectrum plotted in the black line is the spectrum recorded at the output of the polarization maintaining fiber. For more details on the experiments and the simulations, see [73]. *Source*: Suret 2011 [73].

condensation [36, 104–108], whose thermodynamic equilibrium properties are analogous to those of quantum Bose-Einstein condensation [105]. Classical wave condensation can be interpreted as a redistribution of energy among different modes, in which the (kinetic) energy is transferred to small scales fluctuations, while an inverse process increases the power (i.e., number of "particles") into the lowest allowed mode, thus leading to the emergence of a large-scale coherent structure. The phenomenon of condensation has been recently interpreted within a broader perspective in different active and passive optical cavity configurations [109–116]. This raises important questions, such as e.g., the relation between laser operation and the phenomenon of Bose-Einstein condensation. As a matter of fact, these questions are still the subject of vivid debate – we refer the reader to [117–119] for some recent discussions on this important problem.

An important analogy with condensation has been also discussed in the dynamics of active mode-locked laser systems in the presence of additive noise source [111,118,120]. On the basis of their previous works [121, 122], the authors showed that the formation of coherent pulses in actively mode-locked lasers exhibits in certain conditions a transition of the laser mode system to a light pulse state that is similar to the Bose-Einstein condensation, in the sense that it is characterized by a macroscopic occupation of the fundamental mode as the laser power is increased. The analysis is based on statistical light-mode dynamics with a mapping between the distribution of the laser eigenmodes to the equilibrium statistical physics of noninteracting bosons in an external potential. Another analogy with condensation has been pointed out to interpret the radiation emitted by a random laser system in [109]. In this work, the analogy with condensation is supported by the fact that the random laser linewidth is ruled by a nonlinear differential equation, which is the equivalent of the Schwalow-Townes law in standard lasers, and is formally identical to the NLS (Gross-Pitaevskii) equation with a trapping potential.

12.2.3.1 Wave Turbulence in Raman Fiber Lasers

The dynamics of Raman fiber lasers have been also shown to exhibit some interesting analogies with condensation-like phenomena [110, 115, 116]. Here we discuss in more detail these systems in light of the WT theory that has been developed to describe their turbulent dynamics. For more details, we refer the interested reader to [114] for an overview on the WT description of Raman fiber lasers (also see the more recent work [123]).

In [124], the Raman fiber laser is modeled as a turbulent system whose optical power spectrum results from a weakly nonlinear interaction among the multiple modes of the cavity. Performing a mean field approach in which the Raman Stokes field does not evolve significantly over one cavity round trip, the authors of [124] first establish a differential equation for the evolution of the complex amplitude E_n of the nth longitudinal mode

$$\tau_{rt}\frac{dE_n}{dt} - \frac{1}{2}(g - \delta_n)E_n(t) = -\frac{i}{2}\gamma L \sum_{l\neq 0} E_{n-l}(t) \times \sum_{m\neq 0} E_{n-m}(t)E^*_{n-m-l}(t)\exp(2i\beta\, ml\Delta^2\, c\, t). \tag{12.12}$$

In their approach, the time evolution of E_n is determined by the Raman gain g, the dispersion of the fiber, the losses δ_n of the fiber and of the cavity mirrors, and the four-wave mixing process. γ is the Kerr coupling coefficient and β represents the second-order dispersion coefficient of the cavity fiber. $\Delta = 1/\tau_{rt} = c/2L$ is the free spectral range of the Fabry-Perot cavity that has a length L. Gain, losses and dispersive effects occurring inside the whole laser cavity are supposed to influence the formation of the optical power spectrum through their dependence in frequency-space. In particular, fiber Bragg grating mirrors are considered as spectral filters introducing parabolic losses in frequency space ($\delta_n = \delta_0 + \delta_2(n\Delta)^2$). Dispersive effects occurring inside the laser cavity are supposed to be dominantly governed by the second-order dispersion β of the cavity fiber. It must be emphasized that Eq. (12.12) refers to the discretized version of the one-dimensional NLS equation, in which gain and losses terms have been added [125]. In other words, the approach developed by the authors of [124] amounts to apply a WT treatment to a one-dimensional NLS equation, whose integrability is broken by the presence of gain and loss terms.

Assuming an exponential decay for the correlation function among the modes, $\langle E_n(t)E_n^*(t')\rangle = I_n \exp(-|t-t'|/\tau)$, the following WT kinetic equation that governs the temporal evolution of the intracavity spectrum was derived [124]

$$\tau_{rt}\frac{dI(\Omega)}{dt} = (g - \delta(\Omega))I(\Omega) + S_{\mathrm{FWM}}(\Omega), \tag{12.13}$$

where $I(\Omega) = \langle E_n E_n^*\rangle/\Delta$. The mathematical expression of the collision term $S_{\mathrm{FWM}}(\Omega)$ can be separated into two parts

$$S_{\mathrm{FWM}}(\Omega) = -\delta_{\mathrm{NL}} I(\Omega) + (\gamma L)^2 \int \frac{\mathcal{F}[I]\, d\Omega_1\, d\Omega_2}{(3\tau_{rt}/\tau)[1 + (4\tau L\beta/3\tau_{rt})^2\Omega_1^2\Omega_2^2]}, \tag{12.14}$$

where the functional reads $\mathcal{F}[I] = I(\Omega-\Omega_1)I(\Omega-\Omega_2)I(\Omega-\Omega_1-\Omega_2)$, while the nonlinear term responsible for four-wave-mixing-induced losses δ_{NL} reads

$$\delta_{\mathrm{NL}} = (\gamma L)^2 \int \frac{\mathcal{G}[I]\, d\Omega_1\, d\Omega_2}{(3\tau_{rt}/\tau)[1 + (4\tau L\beta/3\tau_{rt})^2\Omega_1^2\Omega_2^2]}, \tag{12.15}$$

where $\mathcal{G}[I] = [I(\Omega-\Omega_1) + I(\Omega-\Omega_2)]I(\Omega-\Omega_1-\Omega_2) - I(\Omega-\Omega_1)I(\Omega-\Omega_1)$. A stationary solution of the WT kinetic Eq. (12.13) has been obtained by Babin et al. in [124], which exhibits the following hyperbolic-secant structure, $I(\Omega) = 2I/\big(\pi\Gamma\cosh(2\Omega/\Gamma)\big)$, where Γ is the width of the intracavity laser power spectrum. This analytical solution is in very good agreement with spectra recorded in experiments in which the fiber laser operates well above threshold, in various different configurations, even in regimes in which the mean field approximation should no longer hold [126]. Although the WT approach developed in [124] has undoubtedly provided a new insight into the physics of Raman fiber lasers, some other numerical and experimental works have raised some interesting questions concerning the applicability of the WT approach to the description of the spectral broadening phenomenon. In particular, numerical simulations of the mean field equations introduced in [124] revealed that the shape of the laser optical power spectrum strongly depends on the sign of the second-order dispersion coefficient [110]. This cannot be captured by the WT theory, which is inherently insensitive to the sign of the second-order dispersion parameter. As pointed out in [125, 127], the formation of the Stokes spectrum is also deeply influenced both by dispersive effects and by the spectral shape of the fiber Bragg grating mirrors used to close the laser cavity.

Laminar-Turbulent Transition in Raman Fiber Lasers Fast recording techniques have recently been exploited for the experimental characterization of a laminar-turbulent transition in Raman fiber lasers [116]. The fiber laser used in these experiments has been specifically designed. It is made with dispersion-free ultra-wideband super-Gaussian fiber grating mirrors. Slightly changing the pump power, an abrupt transition with a sharp increase in the width of laser spectrum has been observed, together with an abrupt change of the statistical properties of the Stokes radiation. The laminar state observed before the transition is associated with a multimode Stokes emission with a relatively narrow linewidth and relatively weak fluctuations of the Stokes power. On the other hand, the turbulent state corresponds to a high multimode operation with a wider spectrum and stronger fluctuations of the Stokes power. The laminar-turbulent transition has been also studied by means of intensive numerical simulations (see Figure 12.8 and [110, 115, 116]). The simulations reveal that, by increasing the pump power, the mechanism underlying the laminar-turbulent transition relies on the generation of an increasing number of dark (or gray) solitons. This experimental work opens new fields of investigations, in particular as regard the impact of phase-defects on the turbulent dynamics of purely 1D wave systems.

Wave Kinetics of Random Fiber Lasers Random lasers are a rapidly growing field of research, with implications in soft-matter physics, light localization, and photonic devices [27, 128, 129]. Considering a different perspective, the authors of [123] described

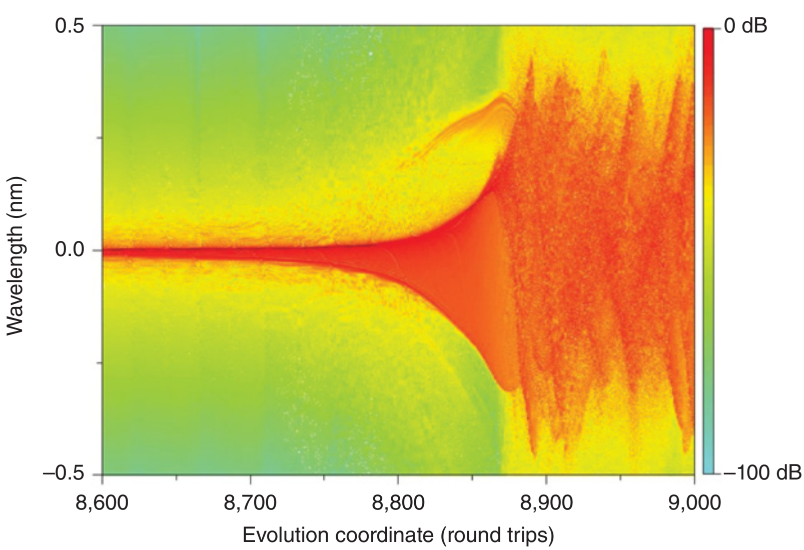

Figure 12.8 Numerical simulations evidencing the laminar-turbulent transition in a Raman fiber laser. The evolution of the laser optical power spectrum is plotted as a function of number of round trips inside the laser cavity. *Source*: Turitsyna 2013 [116]. Reproduced with permission of Nature Publishing Group.

the cyclic wave dynamics inherent to laser systems by considering weakly dissipative modifications of the integrable NLS equation. In this way, a “local kinetic equation” describing the turbulent dynamics of a random fiber laser system is derived [123]. The key property of this kinetic equation is that the $\delta-$function reflecting energy conservation at each elementary four-wave interaction is replaced by an effective Lorentzian function that involves a frequency dependent gain. As a remarkable result, the collision term of the local kinetic equation does not vanish in spite of the trivial resonant conditions inherent to the 1D four-wave interaction with a purely quadratic dispersion relation (see Section 12.2.2.3). From this point of view, the local kinetic equation exhibits properties reminiscent of those considered in [38, 130], although the equations are different, e.g., as regard the renormalization of the dispersion relation by the nonlinearity and the additional nonlinear damping. Then at variance with the purely conservative (Hamiltonian) system, in active cyclic laser systems, the interactions are mediated by a non-homogenous gain, which leads to an effective interaction over the finite interval of the evolution coordinate. We also note that the local kinetic equation is derived under a double separation of scales, i.e., the turbulent regime is dominated by dispersive effects as compared to gain effects, and the gain itself is much larger than gain variation over the typical spectral width of the radiation. Furthermore, the authors confirm their theoretical work by means of direct experimental measurements in random fibre lasers: In the high-power regime, the equilibrium spectrum of the random laser measured experimentally is found in good agreement with the nonequilibrium stationary solution of the local kinetic equation, see Figure 12.9 in the color plate section. Finally, the theory is also completed by means of a generalization of the linear kinetic Schawlow-Townes theory. For more details, we refer the reader to [123].

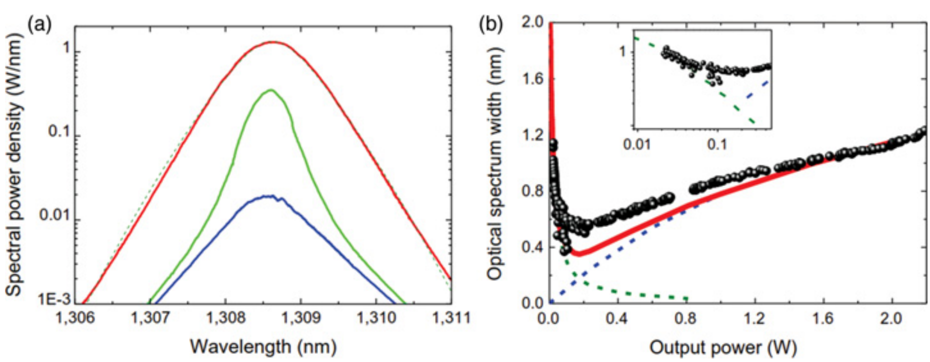

Figure 12.9 Nonlinear kinetic description of the random fiber laser optical spectrum. (a) Optical spectrum measured experimentally: near the generation threshold (blue curve, laser power = 0.025W), slightly above the generation threshold (green curve, 0.2W) and well above the generation threshold (red curve, 1.5W). The optical spectrum predicted by the local wave kinetic equation, for laser power 1.5W is shown by dashed red line. (b) Spectrum width as a function of the laser's output power in theory and experiment. Experimental data are shown by black circles. The prediction for the spectrum broadening from the nonlinear kinetic theory based on the local wave kinetic equation (blue dashed line). The prediction for the spectral narrowing from the modified linear kinetic Schawlow-Townes theory (dashed green line). The red line denotes the sum of nonlinear and linear contributions. The inset shows the spectral narrowing near the threshold in log-scale. For more details see [123].
Source: Churkin 2015 [123]. Reproduced with permission of Nature Publishing Group. For a color version of this figure please see color plate section.

12.2.3.2 Turbulent Dynamics in Passive Optical Cavities

As commented above, a classical wave can exhibit a genuine process of wave condensation as it propagates in a 2D conservative Kerr material, [36, 105, 107]. Actually, a phenomenon completely analogous to such conservative condensation process can occur in an incoherently pumped passive optical cavity, despite the fact that the system is inherently dissipative [113]. For this purpose, let us consider a *passive optical cavity* pumped by an incoherent optical wave, whose time correlation, t_c, is much smaller than the round trip time, $t_c \ll \tau_{rt}$. In this way, the optical field from different cycles are mutually incoherent with one another, which makes the optical cavity *non-resonant*. Because of this property, the cavity does not exhibit the widely studied dynamics of pattern formation [131, 132]. Instead, the dynamics of the cavity exhibit a turbulent behavior that can be characterized by an irreversible process of thermalization toward energy equipartition. A mean-field WT equation was derived in [113], which accounts for the incoherent pumping, the nonlinear interaction and both the cavity losses and propagation losses. In spite of the dissipative nature of the cavity dynamics, the intracavity field undergoes a condensation process below a critical value of the incoherence (kinetic energy) of the pump. This phenomenon is illustrated in Figure 12.10 (a), which shows the temporal evolution of the condensate fraction in the intracavity field: After a transient, the fraction of power condensed in the fundamental transverse mode of the cavity saturates to a constant value, which is found in agreement with the theory. Figure 12.10 (b) reports the condensation curve, i.e., the fraction of condensed power at equilibrium vs the kinetic energy of the injected pump wave. This latter quantity reflects the degree of coherence of the pump wave and plays the role of the control parameter of the transition to wave condensation in the cavity configuration. We remark in Figure 12.10 (b) that the condensate fraction in this dissipative optical cavity is found in agreement with the theory inherited from the conservative Hamiltonian NLS equation, without using adjustable

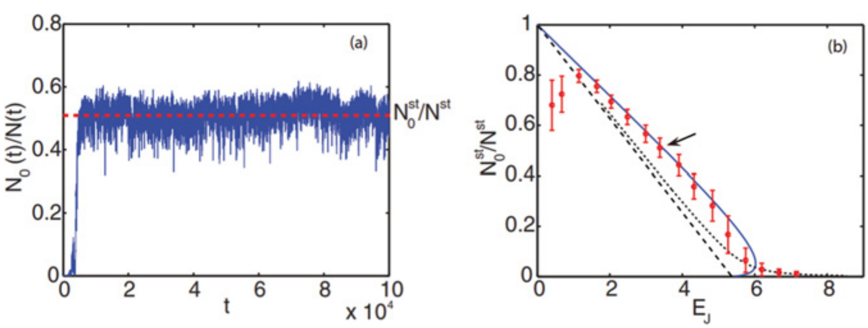

Figure 12.10 Wave condensation in an incoherently pumped passive optical cavity. (a) Evolution of the fraction of condensed power $N_0(t)/N(t)$ vs time t: The condensate growth saturates to a constant value N_0^{st}/N^{st}, which is in agreement with the theory [113]. (b) Condensation curve: fraction of condensed power in the stationary equilibrium state N_0^{st}/N^{st} vs the kinetic energy of the pump E_J. The condensation curve is computed for a fixed value of the pump intensity J_0, while E_J is varied by modifying the degree of coherence of the pump (i.e., its spectral width). The solid line refers to the (Bogoliubov) strong condensation regime. The dotted line refers to the weak condensation regime beyond the thermodynamic limit ($\mu \neq 0$), while the dashed line refers to the thermodynamic limit ($\mu \to 0$). The points correspond to the NLS numerical simulations with the cavity boundary conditions. For more details, see [113]. *Source*: Michel 2011 [113]. Reproduced with permission of American Physical Society.

parameters. For more detail on the simulations and the theory, we refer the reader to [113].

Let us note an important difference that distinguishes the thermalization and condensation processes discussed here with those reported in the quantum photon context in [112, 133]. In these works the thermalization process is achieved thanks to the presence of dye molecules, which thus play the role of an external thermostat. Conversely, in the passive cavity configuration considered here, the process of thermalization solely results from the four-wave interaction mediated by the intracavity Kerr medium, while the "temperature" is controlled by varying the kinetic energy (degree of coherence) of the injected pump.

In a recent experimental work [134], the incoherently pumped passive cavity has been implemented in a fully integrated optical fiber system, close to the zero-dispersion wavelength of the fiber. The dynamics of the cavity exhibit a quasi-soliton turbulent behavior which is reminiscent of the turbulent dynamics of the purely Hamiltonian wave system considered in [135,136]. The analysis reveals that, as the coherence of the injected pump wave is degraded, the cavity undergoes a transition from the coherent quasi-soliton regime toward the highly incoherent (weakly nonlinear) turbulent regime characterized by short-lived and extreme rogue wave events. This transition can then be interpreted by analogy with a phenomenon of quasi-soliton condensation. The experiments realized in the incoherently pumped passive optical cavity have been characterized by means of complementary spectral and temporal PDF measurements [134].

An unexpected result of [134] is that quasi-soliton condensation can take place efficiently, even in the presence of a low cavity finesse, in contrast to wave-condensation in 2D defocusing media discussed here above, which requires a high finesse [113]. This can be interpreted as a consequence of the fact that the process of thermalization of an optical wave constitutes a prerequisite for the phenomenon of wave-condensation in a defocusing medium, while wave thermalization is known to require a high cavity finesse. There is another important difference which distinguishes wave-condensation and (quasi-)soliton condensation. Wave-condensation is known to exhibit a property of long-range order and coherence, in the sense that the correlation function of the field amplitude does not decay at infinity, $\lim_{|\mathbf{r}-\mathbf{r}'|\to\infty}\langle A(\mathbf{r})\, A^*(\mathbf{r}')\rangle \neq 0$, a property consistent with the idea that the coherence length of a plane-wave diverges to infinity [105]. This is in contrast with the spatial localized character of a (quasi-)soliton, which naturally limits the range of coherence to the characteristic spatial width of the (quasi-)soliton structure. Wave-condensation then appears to be more sensitive to the "boundary conditions" of the system, and thus is less robust than (quasi-) soliton condensation when considered in an optical cavity system. The understanding of this aspect requires further investigation.

12.3 Weak Langmuir Turbulence Formalism

In this section we study the temporal evolution of a partially coherent wave that propagates in a nonlinear medium characterized by a noninstantaneous response. As discussed in Section 12.1 through Figure 12.2, a delayed nonlinearity leads to a kinetic description which is formally analogous to the weak Langmuir turbulence kinetic equation, irrespective of the nature of the fluctuations that may be either stationary or non-stationary. In the presence of a temporal long-range response and a stationary statistics of the incoherent wave, the weak Langmuir turbulence formalism reduces to a family of singular integro-differential kinetic equations (e.g., Benjamin-Ono equation) that describe incoherent dispersive shock waves and incoherent collapse singularities in the spectral evolution of the random wave.

12.3.1 NLS Model

A typical example of noninstantaneous nonlinear response in one dimensional systems is provided by the Raman effect in optical fibers [71]. We consider the standard 1D NLS equation to account for a noninstantaneous nonlinear response function

$$i\partial_z\psi + \beta\partial_{tt}\psi + \gamma\psi \int_{-\infty}^{+\infty} R(t-t')\,|\psi|^2(z,t')\,dt' = 0, \tag{12.16}$$

where the response function $R(t)$ is constrained by the causality condition. In the following we use the convention that $t > 0$ corresponds to the leading edge of the pulse, so that the causal response will be on the trailing edge of a pulse, i.e., $R(t) = 0$ for $t > 0$. We will write the response function in the form $R(t) = H(-t)\bar{R}(-t)$, where $\bar{R}(t)$ is a smooth function from $[0,\infty)$ to $(-\infty,\infty)$, while the Heaviside function $H(-t)$ guarantees the causality property. As we will see, this convention will allow us to easily compare the dynamics of temporal and spatial incoherent solitons. Because of the causality property, the real and imaginary parts of the Fourier transform of the response function

$$\tilde{R}(\omega) = \tilde{U}(\omega) + i g(\omega), \tag{12.17}$$

are related by the Kramers-Krönig relations. We recall that $\tilde{U}(\omega)$ is even, while the gain spectrum $g(\omega)$ is odd. The causality condition breaks the Hamiltonian structure of the NLS equation, so that Eq. (12.16) only conserves the total power ("number of particles") of the wave $\mathcal{N} = \int |\psi|^2(t,z)\,dt$. The typical temporal range of the response function $R(t)$ denotes the response time, τ_R. Note that $\beta = -\frac{1}{2}\partial^2_\omega k(\omega)$ in Eq. (12.16), so that $\beta > 0$ ($\beta < 0$) denotes the regime of anomalous (normal) dispersion.

12.3.2 Short-Range Interaction: Spectral Incoherent Solitons

The dynamics are ruled by the comparison of the response time, τ_R, with the 'healing time', $\tau_0 = \sqrt{|\beta| L_{nl}}$. We note that the weakly nonlinear regime of interaction refers to the regime in which linear dispersive effects dominate nonlinear effects, i.e., $L_d/L_{nl} \ll 1$ where $L_d = t_c^2/|\beta|$ and $L_{nl} = 1/(|\gamma|\rho)$ refer to the dispersive and nonlinear characteristic lengths respectively, t_c being the correlation time of the partially coherent wave. We consider here the case of a noninstantaneous nonlinearity characterized by a short-range response time, i.e., $\tau_R \sim \tau_0$. In this regime, it can be shown that the kinetic equation governing the evolution of the incoherent wave takes a form analogous to the WT Langmuir kinetic equation [23, 37]:

$$\partial_z n_\omega(z) = \frac{\gamma}{\pi}\, n_\omega(z) \int_{-\infty}^{+\infty} g(\omega-\omega')\, n_{\omega'}(z)\, d\omega', \tag{12.18}$$

where we have implicitly assumed that the incoherent wave exhibits fluctuation that are statistically stationary (homogeneous) in time—a generalized WT Langmuir equation can be obtained for a non-stationary statistics [37]. We first note that this equation does not account for dispersion effects (it does not involve the parameter β), although the role of dispersion in its derivation is essential in order to verify the criterion of weakly nonlinear interaction, $L_d/L_{nl} \ll 1$. The fact that the dynamics ruled by the WT Langmuir equation do not depend on the sign of the dispersion coefficient has been verified by direct numerical simulations of the NLS Eq. (12.16) [48]. The kinetic Eq. (12.18) conserves the power of the field $N = \frac{1}{2\pi} \int n_\omega(z)\, d\omega$. Moreover, as discussed above for the Vlasov equation, the WT Langmuir Eq. (12.18) is a formally reversible equation [it is invariant under the transformation $(z, \omega) \to (-z, -\omega)$], a feature which is consistent with the fact that it also conserves the non-equilibrium entropy $S = \frac{1}{2\pi} \int \log[n_\omega(z)]\, d\omega$.

The WT Langmuir equation admits solitary wave solutions [23, 47, 48, 54]. This may be anticipated by remarking that, as a result of the convolution product in (12.18), the odd spectral gain curve $g(\omega)$ amplifies the low-frequency components of the wave at the expense of the high-frequency components, thus leading to a global red-shift of the spectrum. We note that these incoherent solitons are termed “spectral” because they can only be identified in the spectral domain, since in the temporal domain the field exhibits stochastic fluctuations at any time, t.

12.3.2.1 Numerical Simulations

Typical spectral incoherent soliton behaviors are reported in Figure 12.11. The initial condition is an incoherent wave characterized by a Gaussian spectrum with $\delta-$correlated random spectral phases, so that the initial wave exhibits stationary fluctuations. The Gaussian spectrum is superposed on a background of small noise of averaged intensity $n_0 = 10^{-5}$. This is important in order to sustain a steady soliton propagation, otherwise the soliton undergoes a slow adiabatic reshaping so as to adapt its shape to the local value of the noise background. The relative intensity of the background noise with respect to the average power of the wave plays an important role in the dynamics of discrete spectral incoherent solitons. Indeed, the *continuous* spectral incoherent soliton is known to become narrower (i.e., of higher amplitude) as the intensity of the background noise decreases. Accordingly, a transition from a continuous to a discrete spectral incoherent soliton behavior occurs as the relative intensity of the background noise is decreased: as the spectral soliton becomes narrower than ω_R, the leading edge of the tail of the spectrum will be preferentially amplified, thus leading to the formation of a discrete spectral incoherent soliton. In order to test the validity of the WT Langmuir theory, we reported in Figure 12.11 a direct comparison with NLS simulations. We emphasize that an excellent agreement has been obtained between the simulations of the NLS equation and the WT Langmuir equation, without using any adjustable parameter [48].

Note that if the background noise level increases in a significant way and becomes of the same order as the amplitude of the spectral soliton, the incoherent wave enters a novel regime [137]. This regime is characterized by an oscillatory dynamics of the incoherent spectrum which develops within a spectral cone during the propagation. Such spectral dynamics exhibit a significant spectral blueshift, which is in contrast with the expected Raman-like spectral redshift.

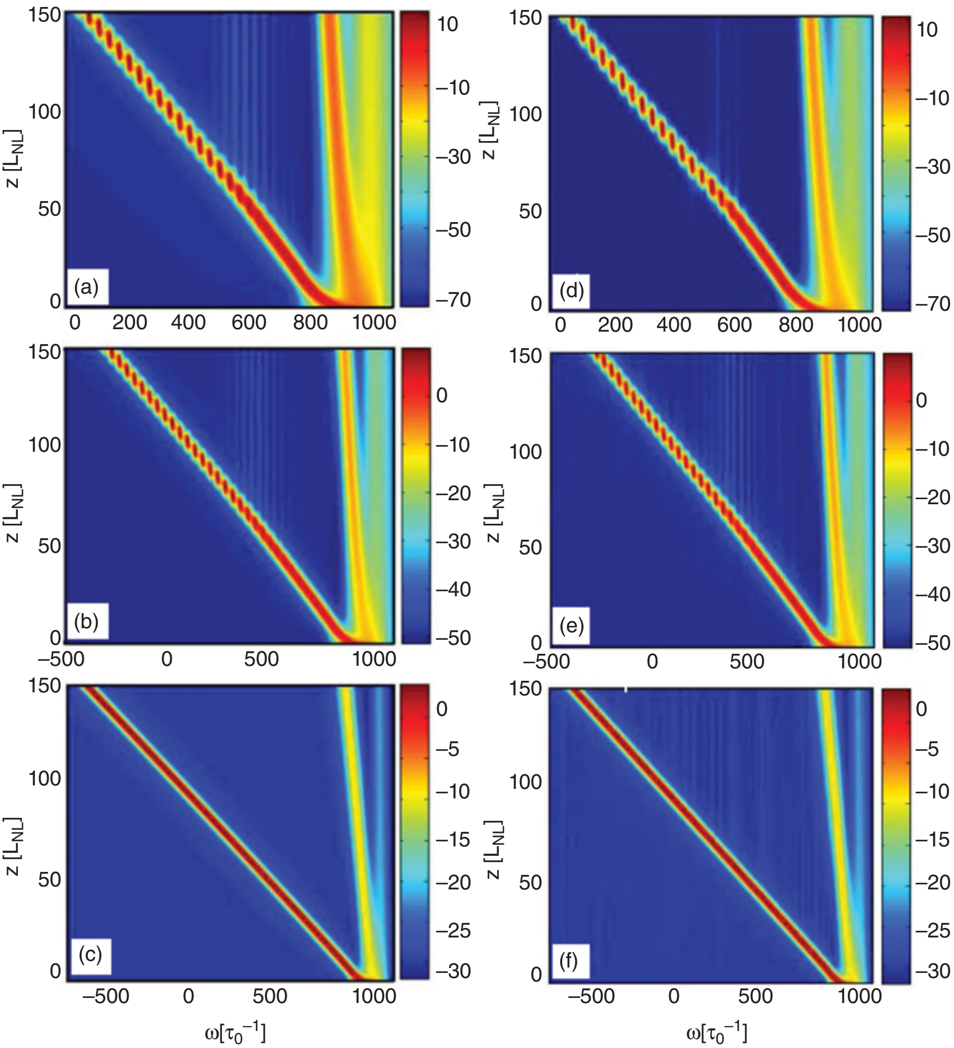

Figure 12.11 Spectral incoherent solitons: Transition from discrete to continuous solitons. Left column (a–c): Evolution of the non-averaged spectrum of the optical field, $|\tilde{\psi}|^2(z,\omega)$ (in dB-scale), obtained by integrating numerically the NLS Eq. (12.16) for three different values of the noise background, $n_0 = 10^{-7}$ (a), $n_0 = 10^{-5}$ (b), $n_0 = 10^{-3}$ (c). Right column (d–f): Corresponding evolution of the averaged spectrum, $n(z,\omega)$ (in dB-scale), obtained by solving the Langmuir WT Eq. (12.18). The comparison reveals a quantitative agreement, without using adjustable parameters. We considered the typical Raman-like gain spectrum, $g(\omega)$ ($\beta\gamma < 0$). *Source*: Michel 2011 [48]. Reproduced with permission of American Physical Society.

12.3.2.2 Analytical Soliton Solution

The WT Langmuir kinetic equation (12.18) admits analytical soliton solutions [37, 54, 138]. More precisely, it is possible to compute the width and velocity of the soliton given its peak amplitude n_m in the regime $n_m \gg n_0$, where n_0 denotes the spectral amplitude of the background noise. We introduce the antiderivative of the spectral gain $G(\omega) = -\int_{\omega}^{\infty} g(\omega')d\omega'$. The gain spectrum $g(\omega)$ is characterized by its typical gain amplitude $g_{\rm i}$ and its typical spectral width $\omega_{\rm i}$. Regardless of the details of the gain curve $g(\omega)$, $g_{\rm i}$ and $\omega_{\rm i}$ can be assessed by two characteristic quantities, namely the gain slope at the origin $\partial_{\omega}g(0)$ and the total amount of gain $G(0) = -\int_0^{\infty} g(\omega)d\omega$. A dimensional analysis allows to express $g_{\rm i}$ and $\omega_{\rm i}$ in terms of these two quantities, $g_{\rm i} = \frac{1}{\sqrt{2}}(-\partial_{\omega}g(0))^{1/2} \big[-\int_0^{\infty} g(\omega)d\omega\big]^{1/2}$, $\omega_{\rm i} = \sqrt{2}\big[-\int_0^{\infty} g(\omega)d\omega\big]^{1/2}/\big[-\partial_{\omega}g(0)\big]^{1/2}$. With these definitions, the function $G(\omega)$ can be written in the following normalized form $G(\omega) = g_{\rm i}\omega_{\rm i}h(\omega/\omega_{\rm i})$, where the dimensionless function $h(x)$ verifies $h(0) = 1$, $h'(0) = 0$, and $h''(0) = -2$. Proceeding as in [138], the profile of the soliton in the regime $n_m \gg n_0$ is of the form [54], $\log\left(\frac{n_{\omega}(z)}{n_0}\right) = \log\left(\frac{n_m}{n_0}\right)h\left(\frac{\omega - Vz}{\omega_{\rm i}}\right)$, or equivalently:

$$n_{\omega}(z) - n_0 = \left(n_m - n_0\right)\exp\left[-\log\left(\frac{n_m}{n_0}\right)\frac{(\omega - Vz)^2}{\omega_{\rm i}^2}\right], \tag{12.19}$$

where the velocity of the soliton is

$$V = -\frac{n_m - n_0}{\log^{3/2}\left(\frac{n_m}{n_0}\right)}\frac{\gamma g_{\rm i}\omega_{\rm i}^2}{\sqrt{\pi}}, \tag{12.20}$$

and its full width at half maximum is $\omega_{\rm sol} = 2\omega_{\rm i}\log^{1/2}(2)/\log^{1/2}(n_m/n_0)$.

Spectral incoherent solitons have recently been generalized in the framework of the generalized NLS equation accounting for the self-steepening term and a frequency dependence of the nonlinear Kerr coefficient [139]. Such nonlinear dispersive effects are shown to strongly affect the dynamics of the incoherent wave. A generalized WT Langmuir kinetic equation is derived and its predictions have been found in quantitative agreement with the numerical simulations of the NLS equation, without adjustable parameters [139].

The structure of discrete spectral incoherent solitons can also be interpreted with an analytical soliton solution of the *discretized* WT Langmuir equation derived in [140]. In this way, discrete frequency bands of the soliton are modelled as coupled Dirac δ-functions in frequency space ($\delta-$peak model). However, the simulations show that, when injected as initial condition into the WT Langmuir equation with a Raman-like gain spectrum, the analytical soliton solution rapidly relaxes during the propagation toward a discrete spectral incoherent solution [48]. This property reveals the incoherent nature of discrete spectral incoherent solitons.

We finally note that the emergence of continuous and discrete spectral incoherent solitons has been identified experimentally owing to the Raman effect in photonic crystal fibers in the context of supercontinuum generation, a feature discussed in detail in [24].

12.3.3 Long-Range Interaction: Incoherent Dispersive Shock Waves

In this section we present the procedure which allows one to derive appropriate reduced kinetic equations from the WT Langmuir equation in the long-range limit, i.e., the limit of a highly noninstantaneous nonlinear response, $\tau_R \gg \tau_0$. As discussed here above, the causality condition leads to a gain spectrum $g(\omega)$ that decays algebraically at infinity, a property which introduces singularities into the convolution operator of the WT Langmuir Eq. (12.18). The mathematical procedure consists in accurately addressing these singularities, see [49]. It reveals that, as a general rule, a singular integro-differential operator arises systematically in the derivation of the reduced kinetic equation [49,141]. The resulting singular integro-differential kinetic equation then originates in the causality property of the nonlinear response function.

These singular integro-differential kinetic equations find a direct application in the description of dispersive shock waves, i.e., shock waves whose singularity is regularized by dispersion effects instead of dissipative (viscous) effects [142] – see Chapter 11 of this book. Dispersive shock waves have been constructed mathematically [143] and observed in ion acoustic waves [144] long ago, though it is only recently that they emerged as a general signature of singular fluid-type behavior in areas as different as Bose-Einstein condensed atoms [145,146], nonlinear optics [90–92,147–149], quantum liquids [150], and electrons [151]. We remark that dispersive shock waves have been also recently studied in the presence of structural disorder of the nonlinear medium [92,152,153].

These previous studies on dispersive shock waves have been discussed for coherent, i.e., deterministic, amplitudes of the waves. Through the analysis of the WT Langmuir equation, we will see that incoherent waves can exhibit dispersive shock waves of a different nature that their coherent counterpart. They manifest themselves as a wave breaking process ("gradient catastrophe") in the spectral dynamics of the incoherent field [49]. Contrary to conventional shocks which are known to require a strong nonlinear regime, these incoherent shocks develop into the weakly nonlinear regime. This WT kinetic approach also reveals unexpected links with the 3D vorticity equation in incompressible fluids [154], or the integrable Benjamin-Ono equation [155], which was originally derived in hydrodynamics, and recently considered in the field of quantum liquids [150].

12.3.3.1 Damped Harmonic Oscillator Response

The derivation of singular integro-differential kinetic equations has been developed for a general form of the response function (see the Supplement of [49]). Here we illustrate the theory by considering two physically relevant examples of response functions, which, respectively, induce and inhibit the formation of incoherent shock waves.

Let us first consider the example of the damped harmonic oscillator response, $\bar{R}(t) = \frac{1+\eta^2}{\eta\tau_R}\sin(\eta t/\tau_R)\exp(-t/\tau_R)$. Figure 12.12 in the color plate section reports a typical evolution of the spectrum of the incoherent wave obtained by numerical simulations of the NLS Eq. (12.16). Here we considered the highly incoherent limit, $\Delta\omega \gg \Delta\omega_g$ ($t_c \ll \tau_R$). We see that the low frequency part of the spectrum exhibits a self-steepening process, whose wave-breaking is ultimately regularized by the development of large amplitude and rapid spectral oscillations typical of a dispersive shock wave. This behavior has been described by deriving a singular integro-differential kinetic equation from the WT Langmuir equation in the long-range regime ($\tau_R \gg \tau_0$):

$$\tau_R^2 \partial_z n_\omega = \gamma(1+\eta^2)\left(n_\omega \partial_\omega n_\omega - \frac{1}{\tau_R} n_\omega \mathcal{H}\partial_\omega^2 n_\omega\right), \tag{12.21}$$

where the singular operator $\mathcal{H}$ refers to the Hilbert transform, $\mathcal{H}f(\omega) = \frac{1}{\pi}\mathcal{P}\int_{-\infty}^{+\infty} \frac{f(\omega-u)}{u} du$, where we recall that $\mathcal{P}$ denotes the Cauchy principal value. This kinetic

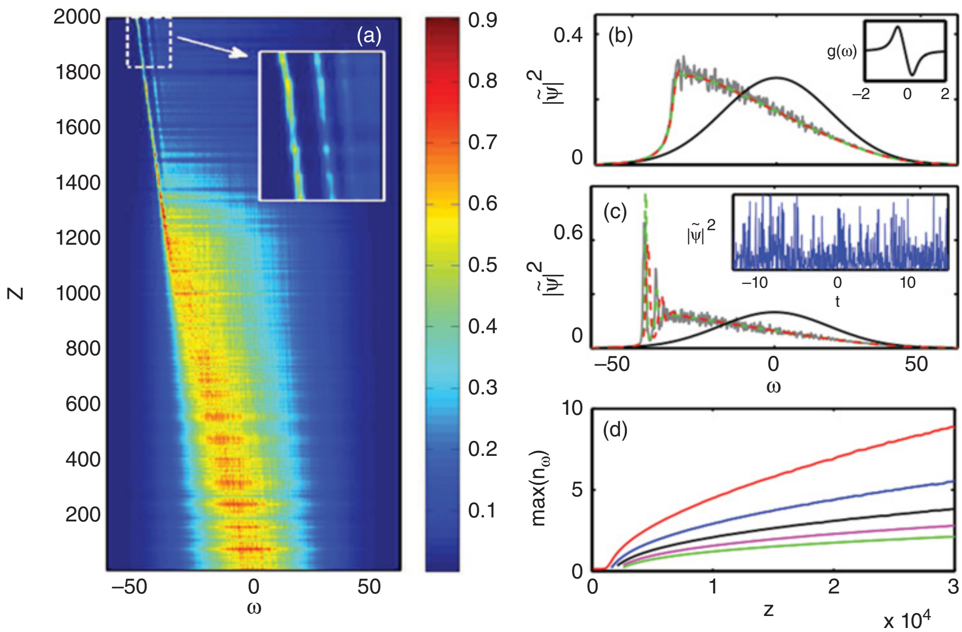

Figure 12.12 Incoherent dispersive shock waves with a Raman-like response function: (a) Numerical simulation of the NLS Eq. (12.16): The stochastic spectrum $|\tilde{\psi}|^2(\omega, z)$ develops an incoherent shock at $z \simeq 1200L_{nl}$ ($\tau_R = 3\tau_0, \eta = 1$). Snapshots at $z = 1040L_{nl}$ (b), $z = 1400L_{nl}$ (c): NLS (12.16) (gray) is compared with WT Langmuir Eq. (12.18) (green), singular kinetic equation (Eq. (12.21)) (dashed line), and initial condition (solid black). (d) First five maxima of n_ω vs z in the long-term post-shock dynamics: the spectral peaks keep evolving, revealing the non-solitonic nature of the incoherent dispersive shock wave. Insets: (b) gain spectrum $g(\omega)$, note that $\Delta\omega_g$ is much smaller than the initial spectral bandwidth of the wave [black line in (b)]. (c) corresponding temporal profile $|\psi(t)|^2$ showing the incoherent wave with stationary statistics. *Source*: Garnier 2013 [49]. Reproduced with permission of American Physical Society. For a color version of this figure please see color plate section.

equation describes the essence of incoherent dispersive shock waves: The leading-order Burgers term describes the formation of the shock, which is subsequently regularized by the nonlinear dispersive term involving the Hilbert operator. We note in Figure 12.12 that a quantitative agreement is obtained between the simulations of Eq. (12.21) and those of the NLS and WT Langmuir equations, without adjustable parameters. Also note that in the presence of a strong spectral background noise, the derived singular equation coincides with the Benjamin-Ono equation, which is a completely integrable equation [49].

12.3.3.2 Exponential Response: Spectral Collapse Singularity

As described by the general theory reported in [49], the previous scenario of incoherent dispersive shock waves changes in a dramatic way when the response function is not continuous at the origin, as it occurs for a purely exponential response function, $\bar{R}(t) = \exp(-t/\tau_R)/\tau_R$. In this case, considering the limit $\tau_R/\tau_0 \gg 1$, the singular kinetic equation takes the form:

$$\tau_R \partial_z n_\omega = -\gamma n_\omega \mathcal{H} n_\omega - \frac{\gamma}{\tau_R} n_\omega \partial_\omega n_\omega + \frac{\gamma}{2\tau_R^2} n_\omega \mathcal{H} \partial_\omega^2 n_\omega. \tag{12.22}$$

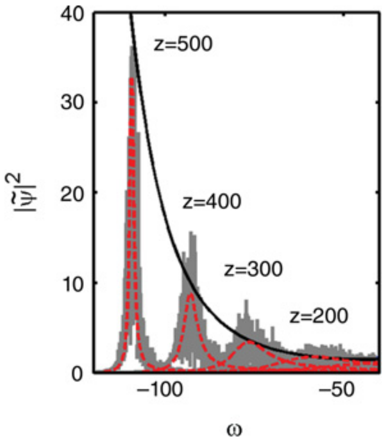

Figure 12.13 Inhibition of incoherent shocks with an exponential response function. Without background spectral noise the spectrum exhibits a collapse-like behavior: NLS (12.16), gray; singular kinetic Eq. (12.22), dashed ($\tau_R = 5\tau_0$). The dark continuous line denotes the theoretical behavior $\sim 1/[z^2 n^0(\omega = \tilde{c}z)]$, with $\tilde{c} = -\gamma N/\tau_R$, predicted from the first term of Eq. (12.22) and the corresponding analytical solution Eq. (12.23).
Source: Garnier 2013 [49]. Reproduced with permission of American Physical Society.

Interestingly, the first term of Eq. (12.22) was considered as a one-dimensional model of the vorticity formulation of the 3D Euler equation of incompressible fluid flows [154]. In this work, the authors found an explicit analytical solution to the equation $\tau_R \partial_z n_\omega = -\gamma n_\omega \mathcal{H} n_\omega$. For a given initial condition $n_\omega(z=0) = n^0_\omega$ the solution has the form

$$n_\omega(z) = \frac{4n^0_\omega}{\left(2 + (\gamma z/\tau_R)\mathcal{H}n^0_\omega\right)^2 + (\gamma z/\tau_R)^2 (n^0_\omega)^2}. \tag{12.23}$$

There is blow up if and only if there exists ω such that $n^0_\omega = 0$ and $\mathcal{H}n^0_\omega < 0$. Then the blow up distance z_c is given by $z_c = -2\tau_R/[\gamma \mathcal{H} n^0_{\omega=\omega_0}]$, where ω_0 is such that $n^0_{\omega_0} = 0$. It can be shown [49] that, if the initial condition decays faster than a Lorentzian, the spectrum exhibits a collapse-like dynamics, which is ultimately arrested by a small background noise. In this process, the spectrum moves at velocity $\tilde{c}$, while its peak amplitude increases according to $\sim 4\tau_R^2/[\gamma^2 z^2 n^0(\omega = \tilde{c}z)]$. This property is confirmed by the simulations of the NLS equation, as illustrated in Figure 12.13.

Impact of Self-Steepening The previous results of incoherent spectral singularities have been recently extended by considering the generalized NLS equation accounting for the self-steepening term [141]. The analysis reveals that self-steepening significantly affects the spectral singularities: (i) It leads to a delay in the development of incoherent dispersive shocks, and (ii) it arrests the incoherent collapse singularity. Furthermore, the spectral collapse-like behavior can be exploited to achieve a significant enhancement (by two orders of magnitudes) of the degree of coherence of the optical wave as it propagates in the fiber.

12.4 Vlasov Formalism

In Section 12.3.3, we considered the role of long-range temporal responses for an incoherent wave characterized by a stationary (homogeneous) statistics. In this section we consider statistically non-stationary random waves in the presence of a highly noninstantaneous nonlinear response, $\tau_R \gg \tau_0$. As discussed in the introductory section (see

Figure 12.2), in this regime, the dynamics of the incoherent wave is ruled by a completely different Vlasov-like formalism. This formalism models the incoherent wave as an ensemble of particles that evolve in a reduced phase-space (i.e., spectrogram), (t, ω). The corresponding particle density is obtained from a Wigner-like transform of the auto-correlation function of the field, $n_\omega(t,z) = \int B(t,\tau,z)\, \exp(i\omega\tau)\, d\tau$, where $B(t,\tau,z) = \langle \psi(t-\tau/2,z)\psi^*(t+\tau/2,z)\rangle$. Starting from the NLS Eq. (12.16) and considering a highly noninstantaneous nonlinear response, the temporal long-range Vlasov kinetic equation takes the form [14,37,156]:

$$\partial_z n_\omega(t,z) + \partial_\omega \tilde{k}_\omega(t,z)\, \partial_t n_\omega(t,z) - \partial_t \tilde{k}_\omega(t,z)\, \partial_\omega n_\omega(t,z) = 0, \tag{12.24}$$

where the generalized dispersion relation reads

$$\tilde{k}_\omega(t,z) = k(\omega) + V(t,z), \tag{12.25}$$

with $k(\omega) = \beta\omega^2$ and the effective potential

$$V(t,z) = -\gamma \int R(t-t')N(t',z)\, dt'. \tag{12.26}$$

The intensity profile of the incoherent wave is $N(t,z) = B(t,\tau=0,z) = (2\pi)^{-1} \int n_\omega(t,z)\, d\omega$. Equation (12.24) conserves $\mathcal{N} = (2\pi)^{-1} \iint n_\omega(t,z) d\omega dt$, and more generally $\mathcal{M} = \iint f[n] d\omega dt$ where $f[n]$ is an arbitrary functional of n. Because of the causality property of $R(t)$, Eq. (12.24) is no longer Hamiltonian [37]. As a consequence, the incoherent wave-packet exhibits a spectral shift, as revealed by the analysis of the total momentum, $\mathcal{P}(z) = (2\pi)^{-1} \iint \omega\, n_\omega(t,z)\, dt\, d\omega$, which is related to the barycenter of the spectrum, $\langle\omega\rangle = \mathcal{P}/\mathcal{N}$. An equation for the momentum can easily be obtained from the Vlasov Eq. (12.24)

$$\partial_z \mathcal{P}(z) = \int V_G(t,z)\, \partial_t N(t,z)\, dt, \tag{12.27}$$

where $V_G(t,z) = -\gamma \int G(t-t')N(t',z)\, dt'$ and $G(t) = \frac{i}{2\pi} \int g(\omega)\, \exp(-i\omega t)\, d\omega$ [37]. Remarking furthermore that $G(t)$ can expressed in terms of the response function, $G(t) = \frac{1}{2}\left[R(t) - R(-t)\right]$, it becomes easy to see that a focusing (defocusing) nonlinearity leads to a spectral red-shift, $\partial_z \mathcal{P} < 0$ (blue-shift, $\partial_z \mathcal{P} > 0$). We can remark that this dependence of the spectral shift on the sign of the nonlinearity is also apparent in the WT Langmuir (see Eq. (12.18)). Note that a spectral blue-shift induced by a defocusing delayed nonlinearity is known to occur, e.g., in plasma [26,157], in which, however, the total power of the wave is no longer conserved (see Chapter 3 in this book).

It is also interesting to analyze the position of the wave-packet in the time domain, $\mathcal{T}(z) = (2\pi)^{-1} \iint t\, n_\omega(t,z)\, dt\, d\omega$, which is related to the barycenter by $\langle t\rangle = \mathcal{T}/\mathcal{N}$. The evolution of $\mathcal{T}(z)$ can easily be obtained from the Vlasov Eq. (12.24)

$$\partial_z \mathcal{T}(z) = 2\beta\mathcal{P}(z), \tag{12.28}$$

so that $\mathcal{T}(z) = \mathcal{T}(0) + 2\beta \int_0^z \mathcal{P}(z')\, dz'$. Accordingly, propagation in the normal (anomalous) dispersion regime in the presence of a focusing (defocusing) nonlinearity leads to an acceleration of the wave-packet toward $t > 0$. Equation (12.28) also reveals that there is a close relation between the spectral shift and the temporal shift of a wave-packet. This can easily be interpreted by remarking that a spectral shift combined with group-velocity dispersion leads to an acceleration of the wave-packet.

12.4.1 Incoherent Modulational Instability

The Vlasov formalism is known to predict the existence of an incoherent MI, a feature which is in some sense an unexpected result. Indeed, as discussed above in this section in the framework of the WT Langmuir formalism, one would expect that a statistically stationary incoherent wave would exhibit a Raman-like spectral red-shift during its propagation. However, a *highly* noninstantaneous response leads to a genuine process of incoherent MI of the wave, which is characterized by the growth of two symmetric MI bands within the spectrum of the incoherent wave [14].

The details of the incoherent MI analysis through a linearization of the long-range Vlasov equation can be found in [14, 37]. In substance, one assumes that the incident field exhibits a stationary statistics, except for small perturbations that depend on t and z. Note that any homogeneous stationary distribution, n_ω^0, is a solution of the Vlasov equation, that is, $\partial_z n_\omega^0 = 0$. Perturbing this stationary solution according to $n_\omega(t,z) = n_\omega^0 + \delta n_\omega(t,z)$, linearizing the Vlasov equation and then solving it by means of a Fourier-Laplace transform, $\tilde{\delta n}_\omega(\Omega,\lambda) = \int_0^\infty dz \int_{-\infty}^{+\infty} dt \, \exp(-\lambda z - i\Omega t)\, \delta n_\omega(t,z)$, gives the following MI growth-rate:

$$\lambda(\Omega) = -2\Delta\omega|\beta\Omega| + |\Omega|\sqrt{2\beta\gamma N_0 \tilde{R}(\Omega)}, \tag{12.29}$$

where we assumed an initial Lorentzian-shaped spectrum, $n_\omega^0 = 2N_0\Delta\omega/(\omega^2 + (\Delta\omega)^2)$ [i.e., $N_0 = (2\pi)^{-1}\int n_\omega^0 d\omega$]. The corresponding incoherent MI gain reads $g_{\rm MI}(\Omega) = 2\Re[\lambda(\Omega)]$. This expression of MI gain is formally analogous to the expression considered in the spatial case, see Eq. (12.28), in [37]. However, because of the causality property of the response function $R(t)$, its Fourier transform is complex, $\tilde{R}(\omega) = \tilde{U}(\omega) + ig(\omega)$. Recalling that $\tilde{U}(\omega)$ is even and $g(\omega)$ odd, the MI gain $g_{\rm MI}(\Omega)$ is always even, which means that incoherent MI is characterized by the growth of two symmetric side-bands. Another consequence of the fact that $\tilde{R}(\omega)$ is complex is that incoherent MI can also occur in the normal dispersion regime, i.e., for $\gamma\beta < 0$ [37].

Difference with Incoherent MI in Instantaneous Response Nonlinear Media We underline that incoherent MI in noninstantaneous nonlinear media is of fundamental different nature with respect to incoherent MI in *instantaneous* media [158]. In the limit $\tau_R \to 0$, incoherent MI can only take place if the spectral width of the incoherent wave is smaller than the MI frequency, $\Delta\omega \ll \omega_{\rm MI}$ [158]. This means that temporal modulations associated to MI are more rapid than the time correlation, $t_c \gg \tau_0$, i.e., MI modulations take place within each individual fluctuation of the incoherent wave. This is in contrast with the incoherent MI discussed here, in which the optimal MI frequency gets much smaller than the spectral bandwidth ($\omega_{\rm MI} \ll \Delta\omega$) as the nonlinearity becomes noninstantaneous, i.e., as τ_R increases. This means that incoherent MI manifests itself by a slow modulation of the whole random wave profile, i.e., the modulation frequency is smaller than the spectral bandwidth, $\omega_{\rm MI} \ll \Delta\omega$. This feature has been confirmed by the numerical simulations of the NLS Eq. (12.16) and the corresponding long-range Vlasov Eq. (12.24) in [14].

12.4.2 Incoherent Solitons in Normal Dispersion

The study of the existence of incoherent soliton states in the temporal domain revealed an unexpected remarkable result [156]. In contrast to a usual soliton, which is known to require a focusing nonlinearity with anomalous dispersion, a highly non-instantaneous nonlinear response leads to incoherent soliton structures which require the inverted situation. In the focusing regime (and anomalous dispersion) the incoherent wave-packet experiences an unlimited spreading, whereas in the defocusing regime (still with anomalous dispersion) the incoherent wave-packet exhibits a self-trapping [156]. This remarkable result has been demonstrated by means of numerical simulations of both NLS and Vlasov equations, and a quantitative agreement has been obtained between them without adjustable parameters. We refer the reader to [156] for details concerning the numerical simulations.

The unexpected existence of localized soliton states in the defocusing regime is explained in detail by the long-range Vlasov Eqs. (12.24)–(12.26). The Vlasov simulations reveal indeed that, after a transient, the wave-packet adopts an invariant profile characterized by a linear spectral shift, which in turn induces a constant IS acceleration (parabolic trajectory) in the temporal domain. More specifically, let us denote by α_0 the soliton velocity in frequency space. As discussed above through Eq. (12.27), the momentum evolves linearly as $\mathcal{P}(z) = \mathcal{N}\alpha_0 z$. Then Eq. (12.28) explicitly shows that, when combined with group-velocity dispersion, this linear spectral shift induces an acceleration of the incoherent soliton in the temporal domain given by Eq. (12.28)

$$\mathcal{T}(z) = \mathcal{T}(0) + \beta\mathcal{N}\alpha_0 z^2. \tag{12.30}$$

Both phenomena of linear spectral shift and constant acceleration of the incoherent soliton are clearly visible in the numerical simulations, as illustrated in Figure 12.14.

- ***Temporal vs Spatial Incoherent Solitons*** To discuss the mechanism underlying the formation of the incoherent soliton, it is instructive to comment first on an analogy with a *nonlocal spatial response*. Contrary to temporal effects, nonlocal spatial effects are not constrained by the causality condition, so that the spatial response function $U(x)$ is even, as well as the self-consistent potential $V(x) = -\gamma U * N$. Then in the focusing regime ($\gamma > 0$), the optical beam induces an attractive potential $V(x) < 0$, so that the beam is guided by its own induced potential. Conversely, in the defocusing regime ($\gamma < 0$) the repelling potential leads to the expected beam spreading, see Figures 12.15 (a) and (b) [22].
- ***Vlasov Approach: Noninertial Reference Frame*** As a result of the causality property of $R(t)$, the self-consistent potential $V(t)$ is shifted toward $t < 0$ in the temporal domain (see Figures 12.15 (c) and (d). Moreover, as commented above through Figure 12.14, the spectral-shift of the wave-packet, with spectral velocity α, leads to a constant acceleration of the IS. It thus proves convenient to study the dynamics of the wave-packet in its own accelerating reference frame, $\xi = z, \quad \tau = t - \alpha\beta z^2, \quad \Omega = \omega - \alpha z$. In this non-inertial reference frame the Vlasov Eq. (12.24) reads $\partial_\xi n_\Omega(\tau,\xi) + 2\beta\Omega\partial_\tau n_\Omega(\tau,\xi) - \partial_\tau V_{\text{eff}}(\tau,\xi)\,\partial_\Omega n_\Omega(\tau,\xi) = 0$. This equation remarkably reveals the existence of an effective self-consistent potential

$$V_{\text{eff}}(\tau,\xi) = V(\tau,\xi) + \alpha\tau, \tag{12.31}$$

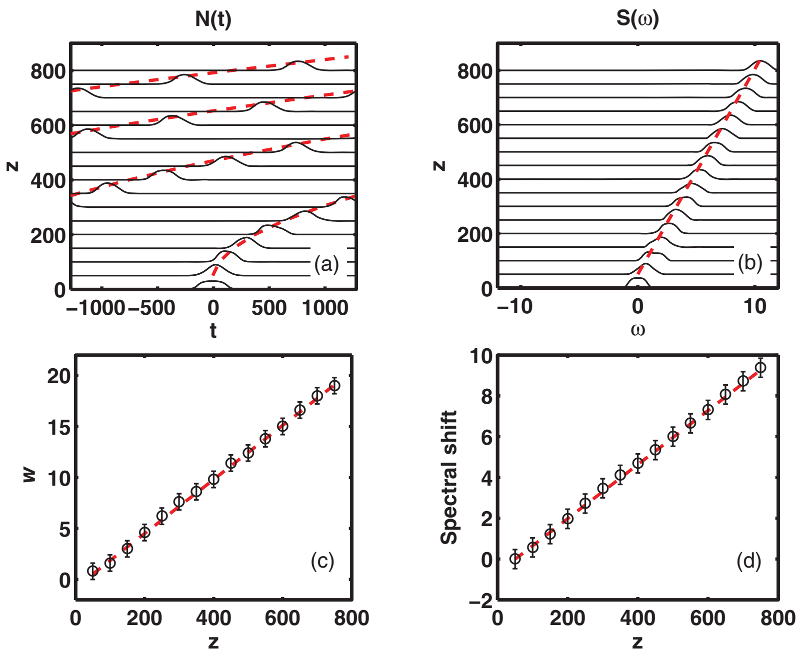

Figure 12.14 Spatial and temporal behaviors of temporal incoherent solitons. The soliton is characterized by a constant acceleration: Parabolic trajectory of the intensity profile $N(t,z) = (2\pi)^{-1} \int n_\omega(t,z)d\omega$ (a), and evolution of the spectral profile $S(\omega,z) = \int n_\omega(t,z)dt$ (b). The linear increase of the incoherent soliton velocity w (constant acceleration) (c), results from the linear spectral shift of the incoherent soliton (d). *Source*: Michel 2012 [156]. Reproduced with permission of American Physical Society.

where $V(\tau,\xi) = -\gamma \int_{-\infty}^{+\infty} R(\tau-\tau')N(\tau',\xi)\,d\tau'$. The linear part of the potential in Eq. (12.31) finds its origin in the fictitious force which results from the non-inertial nature of the reference frame. It is this fictitious force which prevents the IS structure from dispersing toward the direction of increasing τ. Note that this force is analogous to the effective gravity mimicked by an elevator, an analogy that was commented on in [159].

This fictitious force due to the accelerating reference frame explains both phenomena of self-trapping with a defocusing nonlinearity, as well as the inhibition of self-trapping with a focusing nonlinearity. Let us first discuss the defocusing regime. Recalling that the potential is induced by the wave-packet itself, an IS can only form provided that *the self-induced potential* $V_{\text{eff}}(\tau)$ has a local minimum at the pulse center, i.e., at $\tau = 0$ in the accelerating reference frame of the IS. Contrary to the spatial case (Figure 12.15 (a)), it seems that this condition cannot be satisfied in the temporal case, since the causality condition shifts the potentials toward $\tau < 0$. However, in the defocusing regime, a local minimum can be restored at $\tau = 0$ thanks to the fictitious force due to the non-inertial reference frame, as illustrated in Figure 12.15 (d). More precisely, one can Taylor expand the effective potential $V_{\text{eff}}(\tau) = a + (b+\alpha)\tau + c\tau^2 + \mathcal{O}(\tau^3)$ at $\tau = 0$, where $b < 0$ in the defocusing regime and $c > 0$ if the nonlinear response is slow

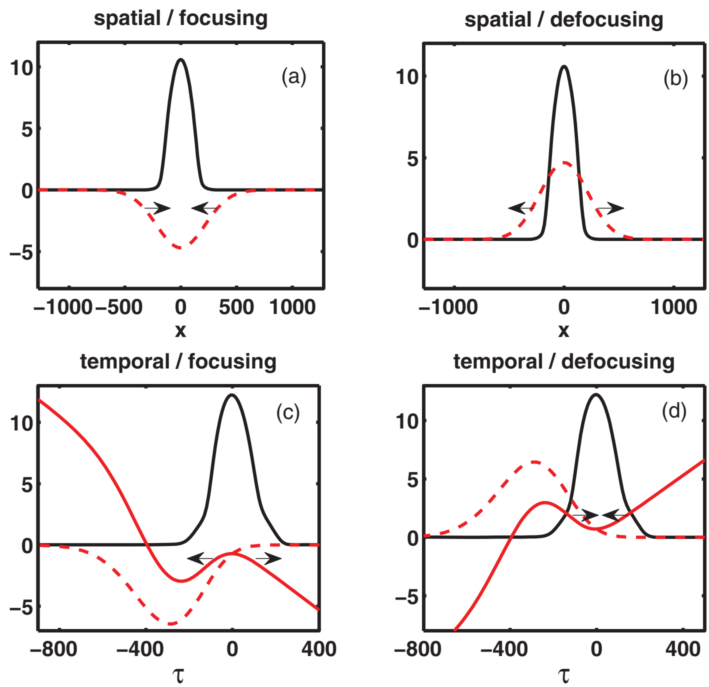

Figure 12.15 Mechanism underlying the formation of temporal incoherent solitons: Intensity profile $N(x)$ (continuous dark line) and corresponding self-consistent potential $V(x) = -\gamma U * N$ (dashed line), in the case of a spatial nonlocal nonlinearity in the focusing (a), and defocusing (b), regimes. Intensity profile $N(\tau)$ obtained by integrating numerically the Vlasov equation (continuous dark line), corresponding self-consistent potential $V(\tau) = -\gamma R * N$ (dashed line), and effective potential $V_{\text{eff}}(\tau)$ [Eq. (12.31)] (continuous line) in the accelerating reference frame, in the case of a temporal noninstantaneous nonlinearity in the focusing (c), and defocusing (d), regimes. The arrows indicate the "particle motions" in the effective self-consistent potentials $V_{\text{eff}}(\tau)$: The non-inertial fictitious force inhibits (c) (induces (d)) the self-trapping in the defocusing (focusing) regime. *Source*: Michel 2012 [156]. Reproduced with permission of American Physical Society.

enough (see Figure 12.15 (d)). In these conditions the particular choice $\alpha_0 = -b$ guarantees that $V_{\text{eff}}(\tau)$ has a local minimum at $\tau = 0$ (see Figure 12.15 (d)). In other words, the system spontaneously selects the amount of spectral shift, $\alpha_0 = -\partial_\tau V|_{\tau=0}$, and hence the amount of soliton acceleration, $2\beta\alpha_0$, in such a way that the effective self-consistent potential $V_{\text{eff}}(\tau)$ admits a local minimum at $\tau = 0$. This is confirmed by the numerical simulations of the Vlasov equation reported in Figure 12.15 (d) (for more details see [156]).

Let us now discuss the focusing regime, which is characterized by a redshift of the wave-packet, $\alpha < 0$. Following the same reasoning as above and remarking that we now have $b > 0$ and $c < 0$, the choice $\alpha_0 = -b$ still leads to an extremum of $V_{\text{eff}}(\tau)$ at $\tau = 0$. However, contrary to the defocusing regime, this extremum refers to a local maximum, as illustrated in Figure 12.15 (c). Actually, in the focusing regime, there is no value of α such that $V_{\text{eff}}(\tau)$ has a local minimum at $\tau = 0$. The local maximum around $\tau = 0$ then plays the role of a repelling potential, which explains the temporal broadening of the incoherent pulse: the "unstable particles" located near by $\tau = 0$ are either attracted toward the local minimum at $\tau < 0$, or either pushed toward $\tau > 0$ by the non-inertial force (see Figure 12.15 (c)). For more details on the dynamics and the interaction of temporal incoherent solitons, we refer the reader to [156, 160].

12.5 Conclusion

In this section we briefly comment on some open interesting issues related to optical wave turbulence in fibers. An interesting problem concerns a proper description of the emergence of extreme rogue waves from a turbulent environment. As discussed in Chapter 10 in this book, a rather commonly accepted opinion is that RWs can be conveniently interpreted in the light of exact analytical solutions of integrable nonlinear wave equations, the so-called Akhmediev breathers, or more specifically their limiting cases of infinite spatial and temporal periods, the rational soliton solutions, such as Peregrine and higher-order solutions of the integrable 1D NLSE – see the recent reviews [30, 31]. Rational soliton solutions can be regarded as a coherent and deterministic approach to the understanding of RW phenomena. On the other hand, RWs are known to spontaneously emerge from an incoherent turbulent state [32, 98, 161–164]. This raises a difficult problem, since the description of the turbulent system requires a statistical WT approach, whereas rational soliton solutions are inherently coherent deterministic structures. This problem was addressed in the optical fiber context in [135, 136] by considering a specific NLSE model that exhibits a quasi-soliton turbulence scenario, a feature that can be interpreted by analogy with wave condensation, see Section 12.2.3.2. It was shown that the deterministic description of rogue wave events in terms of rational soliton solutions is not inconsistent with the corresponding statistical WT description of the turbulent system [136]. It is important to stress that the emergence of RW events was shown to solely occur close to the transition to (quasi-)soliton condensation. From a different perspective, the fluctuations of the condensate fraction in 2D wave condensation have recently been computed theoretically, revealing that large fluctuations solely occur near by the transition to condensation, while they are significantly quenched in the strongly condensed Bogoliubov regime (small "temperature"), and almost completely suppressed in the weakly nonlinear turbulent regime (high "temperature"). This result is consistent with the general idea that nearby second-order phase-transitions, physical systems are inherently sensitive to perturbations and thus exhibit large fluctuations. One can then address a possible alternative point of view on the question of the spontaneous emergence of rogue waves from a conservative turbulent environment: Is it possible to interpret the sporadic emergence of RW events as the natural large fluctuations inherent to the phase transition to soliton condensation? This issue may pave the way for a statistical mechanics approach based on the idea of scaling and universal theory of critical phenomena to the description of RWs.

An other interesting problem concerns a proper statistical description of nonlinear partially polarized optical waves in the framework of the WT theory. In particular, a remarkable phenomenon of nonlinear repolarization without loss of energy is discussed in this book in Chapter 8. This effect of "polarization attraction" has been shown to exhibit different properties depending on the experimental configuration, and on the type of the optical fiber (isotropic, highly birefringent, as well as randomly birefringent fibers), see Chapter 8. Although significant progress has been achieved in order to interpret this phenomenon on the basis of Hamiltonian singularities (see, e.g., [165]), so far, no statistical description has been developed to describe polarization attraction with partially polarized waves. This problem raises important difficulties, since the phenomenon of repolarization is inherently associated to the emergence of a mutual correlation between orthogonal polarization components, while the basic WT theory does not account for such phase-correlation effects. It would be interesting to construct a generalized WT formulation of random nonlinear waves that would account for a possible mutual correlation between distinct incoherent wave components.

Finally, in this chapter we pointed out several remarkable properties of turbulent wave systems that exhibit long-range interactions, by complete analogy with collective behaviors in self-gravitational systems (e.g., formation of galaxies) or 2D geophysical fluids (e.g., Jupiter red hot spot) [56]. Recently, experiments in the spatial domain have been performed in solutions of graphene nano-flakes in which the range of nonlocal interaction can be tuned over more than one order of magnitude. A different experimental setting for the study of long-range wave turbulence in the temporal domain could be hollow-core fibers (see Chapter 3 in this book). Indeed, one may exploit the easily tailorable non-instantaneous response via the well-known Raman effect, as well as other recently investigated mechanisms involving liquid-cores or photo-ionizable noble gases and surface plasmon polaritons [166–168].

Acknowledgments

The authors are grateful to many collaborators for fruitful discussions: P. Aschieri, S.A. Babin, J. Barré, B. Barviau, P. Béjot, F. Biancalana, S. Coen, C. Conti, D. Faccio, C. Finot, M. Guasoni, R. Kaiser, B. Kibler, M. Haelterman, K. Hammani, H.R. Jauslin, M. Lisak, C. Michel, C. Montes, S. Nazarenko, M. Onorato, S. Pitois, E.V. Podivilov, M. Segev, S. Trillo, S. Wabnitz, V.E. Zakharov. The authors also acknowledge P. Suret, S. Randoux, D. Churkin and S. Turitsyn for their deep insights and valuable contributions in the understanding of optical turbulence, in particular in dissipative laser systems or near by the limit of integrability. A.P. is especially grateful to S. Rica for several illuminating discussions on the wave turbulence theory, and to T. Dauxois and S. Ruffo for their introduction to the physics of long-range interactions.

A.P. and G.M. acknowledge support from the French National Research Agency (ANR-12-BS04-0011 OPTIROC), as well as from the Labex ACTION (ANR-11-LABX-01-01) program. A.P. also acknowledges support from the European Research Council under the European Community's Seventh Framework Programme (FP7/20072013 Grant Agreement No. 306633, PETAL project).

References

1 Mitchell, M., Chen, Z., Shih, M., and Segev, M. (1996) Self-trapping of partially spatially incoherent light. *Physical Review Letters*, **77**, 490.

2 Mitchell, M. and Segev, M. (1997) Self-trapping of incoherent white light. *Nature (London)*, **387**, 880.

3 Segev, M. and Christodoulides, D. (2001) Incoherent solitons. In Eds. S. Trillo and W. Torruellas, Spatial Solitons, Springer; Berlin.
4 Kivshar, Y. and Agrawal, G. (2003) *Optical Solitons: From Fibers to Photonic Crystals*, Academic Press, New York.
5 Pasmanik, G.A. (1974) Self-interaction of incoherent light beams. *Soviet Physics JETP*, **39**, 234.
6 Mitchell, M., Segev, Coskun, M.T., and Christodoulides, D. (1997) Theory of self-trapped spatially incoherent light beams. *Physical Review Letters*, **79**, 4990.
7 Christodoulides, D., Coskun, T., Mitchell, M., and Segev, M. (1997) Theory of incoherent self-focusing in biased photorefractive media. *Physical Review Letters*, **78**, 646.
8 Hall, B., Lisak, M., Anderson, D., Fedele, R., and Semenov, V.E. (2002) Statistical theory for incoherent light propagation in nonlinear media. *Physical Review E*, **65**, 035 602.
9 Christodoulides, D.N., Eugenieva, E.D., Coskun, T.H., Segev, M., and Mitchell, M. (2001) Equivalence of three approaches describing partially incoherent wave propagation in inertial nonlinear media. *Physical Review E*, **63**, 035 601.
10 Lisak, M., Helczynski, L., and Anderson, D. (2003) Relation between different formalisms describing partially incoherent wave propagation in nonlinear optical media. *Optics Communications*, **220**, 321.
11 Christodoulides, D.N., Coskun, T.H., Mitchell, M., Chen, Z., and Segev, M. (1998) Theory of incoherent dark solitons. *Physical Review Letters*, **80**, 5113.
12 Chen, Z., Mitchell, M., Segev, M., Coskun, T.H., and Christodoulides, D.N. (1998) Self-trapping of dark incoherent light beams. *Science*, **280**, 889.
13 Soljacic, M., Segev, M., Coskun, T., Christodoulides, D., and Vishwanath, A. (2000) Modulation instability of incoherent beams in noninstantaneous nonlinear media. *Physical Review Letters*, **84**, 467.
14 Kibler, B., Michel, C., Garnier, J., and Picozzi, A. (2012) Temporal dynamics of incoherent waves in noninstantaneous response nonlinear Kerr media. *Optics Letters*, **37**, 2472.
15 Buljan, H., Cohen, O., Fleischer, J.W., *et al.* (2004) Random-phase solitons in nonlinear periodic lattices. *Physical Review Letters*, **92**, 223 901.
16 Cohen, O., Bartal, G., Buljan, H., *et al.* (2005) Observation of random phase lattice solitons. *Nature (London)*, **433**, 500.
17 Picozzi, A. and Haelterman, M. (2001) Parametric three-wave soliton generated from incoherent light. *Physical Review Letters*, **86**, 2010–2013.
18 Picozzi, A., Haelterman, M., Pitois, S., and Millot, G. (2004) Incoherent solitons in instantaneous response nonlinear media. *Physical Review Letters*, **92**, 143 906.
19 Peccianti, M. and Assanto, G. (2001) Incoherent spatial solitary waves in nematic liquid crystals. *Optics Letters*, **26** (22), 1791–1793.
20 Cohen, O., Buljan, H., Schwartz, T., Fleischer, J.W., and Segev, M. (2006) Incoherent solitons in instantaneous nonlocal nonlinear media. *Physical Review E*, **73**, 015 601.
21 Rotschild, C., Schwartz, T., Cohen, O., and Segev, M. (2008) Incoherent spatial solitons in effectively-instantaneous nonlocal nonlinear media. *Nature Photonics*, **2**, 371.
22 Picozzi, A. and Garnier, J. (2011) Incoherent soliton turbulence in nonlocal nonlinear media. *Physical Review Letters*, **107** (23), 233 901.

23 Picozzi, A., Pitois, S., and Millot, G. (2008) Spectral incoherent solitons: A localized soliton behavior in frequency space. *Physical Review Letters*, **101**, 093 901.

24 Kibler, B., Michel, C., Kudlinski, A., *et al.* (2011) Emergence of spectral incoherent solitons through supercontinuum generation in a photonic crystal fiber. *Physical Review E*, **84**, 066 605.

25 Dudley, J.M. and Taylor, J.R. (2010) *Supercontinuum Generation in Optical Fibers*, Cambridge University Press, Cambridge.

26 Couairon, A. and Mysyrowicz, A. (2007) Femtosecond filamentation in transparent media. *Physics Reports*, **441** (2), 47–189.

27 Wiersma, D.S. (2008) The physics and applications of random lasers. *Nature Physics*, **4** (5), 359–367.

28 Akhmediev, N. and Pelinovsky, E. (2010) Editorial–introductory remarks on discussion & debate: Rogue waves–towards a unifying concept. *The European Physical Journal Special Topics*, **185** (1), 1–4.

29 Ruban, V., Kodama, Y., Ruderman, M., *et al.* (2010) Rogue waves–towards a unifying concept: Discussions and debates. *The European Physical Journal Special Topics*, **185** (1), 5–15.

30 Onorato, M., Residori, S., Bortolozzo, U., Montina, A., and Arecchi, F. (2013) Rogue waves and their generating mechanisms in different physical contexts. *Physics Reports*.

31 Dudley, J.M., Dias, F., Erkintalo, M., and Genty, G. (2014) Instabilities, breathers and rogue waves in optics. *Nature Photonics*, **8** (10), 755–764.

32 Walczak, P., Randoux, S., and Suret, P. (2015) Optical rogue waves in integrable turbulence. *Physical Review Letters*, **114**, 143 903.

33 Zakharov, V.E., L'vov, V.S., and Falkovich, G. (1992) *Kolmogorov Spectra of Turbulence I*, Springer; Berlin.

34 Frisch, U. (1995) *Turbulence. The Legacy of A. N. Kolmogorov*, Cambridge: Cambridge University Press.

35 Newell, A.C. and Rumpf, R. (2011) Wave turbulence. *Annual Review of Fluid Mechanics*, **43**, 59–78.

36 Nazarenko, S. (2011) *Wave Trubulence*, Lecture Notes in Physics 825, Springer, Berlin.

37 Picozzi, A., Garnier, J., Hansson, T., *et al.* (2014) Optical wave turbulence: Towards a unified nonequilibrium thermodynamic formulation of statistical nonlinear optics. *Physics Reports*, **542** (1), 1–132.

38 Dyachenko, S., Newell, A.C., Pushkarev, A., and Zakharov, V.E. (1992) Optical turbulence: weak turbulence, condensates and collapsing filaments in the nonlinear Schrödinger equation. *Physica D*, **57**, 96.

39 Zakharov, V., Dias, F., and Pushkarev, A. (2004) One-dimensional wave turbulence. *Physics Reports*, **398**, 1.

40 Benney, D.J. and Saffman, P.G. (1966) Nonlinear interactions of random waves in dispersive medium. *Proceedings of the Royal Society of London Ser. A*, **289**, 301.

41 Benney, D.J. and Newell, A. (1969) Random wave closure. *Studies in Applied Mathematics*, **48**, 29.

42 Newell, A.C., Nazarenko, S., and Biven, L. (2001) Wave turbulence and intermittency. *Physica D*, **152-153**, 520–550.

43 Rumpf, R. and Newell, A.C. (2001) Coherent structures and entropy in constrained, modulationally unstable, nonintegrable systems. *Physical Review Letters*, **87**, 054 102.

44 Rumpf, R. and Newell, A.C. (2003) Localization and coherence in nonintegrable systems. *Physica D*, **184**, 162.

45 Rumpf, B. (2004) Simple statistical explanation for the localization of energy in nonlinear lattices with two conserved quantities. *Physical Review E*, **69**, 016 618.

46 Leuzzi, L., Conti, C., Folli, V., Angelani, L., and Ruocco, G. (2009) Phase diagram and complexity of mode-locked lasers: From order to disorder. *Physical Review Letters*, **102**, 083 901.

47 Musher, S., Rubenchik, A., and Zakharov, V. (1995) Weak Langmuir turbulence. *Physics Reports*, **252**, 177.

48 Michel, C., Kibler, B., and Picozzi, A. (2011) Discrete spectral incoherent solitons in nonlinear media with noninstantaneous response. *Physical Review A*, **83**, 023 806.

49 Garnier, J., Xu, G., Trillo, S., and Picozzi, A. (2013) Incoherent dispersive shocks in the spectral evolution of random waves. *Physical Review Letters*, **111** (11), 113 902.

50 Zakharov, V.E., Musher, S.L., and Rubenchik, A.M. (1985) Hamiltonian approach to the description of non-linear plasma phenomena. *Physics Reports*, **129**, 285.

51 Hasegawa, A. (1975) Dynamics of an ensemble of plane waves in nonlinear dispersive media. *Physics of Fluids*, **18**, 77.

52 Onorato, M., Osborne, A., Fedele, R., and Serio, M. (2003) Landau damping and coherent structures in narrow-banded 1 + 1 deep water gravity waves. *Physical Review E*, **67**, 046 305.

53 Garnier, J., Ayanides, J.P., and Morice, O. (2003) Propagation of partially coherent light with the Maxwell-Debye equation. *Journal of the Optical Society of America B*, **20**, 1409.

54 Garnier, J. and Picozzi, A. (2010) Unified kinetic formulation of incoherent waves propagating in nonlinear media with noninstantaneous response. *Physical Review A*, **81**, 033 831.

55 Dylov, D. and Fleischer, J. (2008) Observation of all-optical bump-on-tail instability. *Physical Review Letters*, **100**, 103 903.

56 Campa, A., Dauxois, T., Fanelli, D., and Ruffo, S. (2014) *Physics of Long-Range Interaction Systems*, Oxford University Press, University.

57 Dudley, J.M., Genty, G., and Coen, S. (2006) Supercontinuum generation in photonic crystal fiber. *Review of Modern Physics*, **78**, 1135.

58 Skryabin, D. and Gorbach, A. (2010) Colloquium: Looking at a soliton through the prism of optical supercontinuum. *Review of Modern Physics*, **82**, 1287.

59 Kolesik, M., Wright, E.M., and Moloney, J.V. (2004) Dynamic nonlinear X-waves for femtosecond pulse propagation in water. *Physical Review Letters*, **92**, 253 901.

60 Kolesik, M., Tartara, L., and Moloney, J.V. (2010) Effective three-wave-mixing picture and first born approximation for femtosecond supercontinua from microstructured fibers. *Physical Review A*, **82**, 045 802.

61 Genty, G., Surakka, M., Turunen, J., and Friberg, A. (2011) Complete characterization of supercontinuum coherence. *Journal of the Optical Society of America B*, **28**, 2301.

62 Erkintalo, M., Surakka, M., Turunen, J., Friberg, A.T., and Genty, G. (2012) Coherent-mode representation of supercontinuum. *Optics Letters*, **37** (2), 169–171.

63 Korhonen, M., Friberg, A.T., Turunen, J., and Genty, G. (2013) Elementary field representation of supercontinuum. *Journal of the Optical Society of America B*, **30** (1), 21–26.

64 Mussot, A., Beaugeois, M., Bouazaoui, M., and Sylvestre, T. (2007) Tailoring cw supercontinuum generation in microstructured fibers with two-zero dispersion wavelengths. *Optics Express*, **15** (18), 11 553–11 563.

65 Martin-Lopez, S., Abrardi, L., Corredera, P., Herraez, M.G., and Mussot, A. (2008) Spectrally-bounded continuous-wave supercontinuum generation in a fiber with two zero-dispersion wavelengths. *Optics Express*, **16** (9), 6745–6755.

66 Cumberland, B.A., Travers, J.C., Popov, S.V., and Taylor, J.R. (2008) 29 w high power cw supercontinuum source. *Optics Express*, **16** (8), 5954–5962.

67 Wadsworth, W., Joly, N., Knight, J., *et al.* (2004) Supercontinuum and four-wave mixing with q-switched pulses in endlessly single-mode photonic crystal fibres. *Optics Express*, **12** (2), 299–309.

68 Barviau, B., Kibler, B., Coen, S., and Picozzi, A. (2008) Towards a thermodynamic description of supercontinuum generation. *Optics Letters*, **33**, 2833.

69 Barviau, B., Kibler, B., Kudlinski, A., *et al.* (2009) Experimental signature of optical wave thermalization through supercontinuum generation in photonic crystal fiber. *Optics Express*, **17**, 7392.

70 Barviau, B., Kibler, B., and Picozzi, A. (2009) Wave turbulence description of supercontinuum generation: influence of self-steepening and higher-order dispersion. *Physical Review A*, **79**, 063 840.

71 Agrawal, G. (2012) *Nonlinear Fiber Optics*, 5th Ed., Academic Press, New York.

72 Soh, D.B.S., Koplow, J.P., Moore, S.W., Schroder, K.L., and Hsu, W.L. (2010) The effect of dispersion on spectral broadening of incoherent continuous-wave light in optical fibers. *Optics Express*, **18** (21), 22 393–22 405.

73 Suret, P., Picozzi, A., and Randoux, S. (2011) Wave turbulence in integrable systems: Nonlinear propagation of incoherent optical waves in single-mode fibers. *Optics Express*, **19**, 17 852.

74 Suret, P., Randoux, S., Jauslin, H., and Picozzi, A. (2010) Anomalous thermalization of nonlinear wave systems. *Physical Review Letters*, **104**, 054 101.

75 Michel, C., Suret, P., Randoux, S., Jauslin, H., and Picozzi, A. (2010) Influence of third-order dispersion on the propagation of incoherent light in optical fibers. *Optics Letters*, **35**, 2367.

76 Pitois, S., Lagrange, S., Jauslin, H.R., and Picozzi, A. (2006) Velocity locking of incoherent nonlinear wave packets. *Physical Review Letters*, **97**, 033 902.

77 Landau, L. and Lifchitz, E. (1980) *Statistical Physics*, Pergamon Press, New York, Part 1.

78 Gallavotti, G.E. (2007) *The Fermi-Pasta-Ulam Problem: A Status Report*, Lecture Notes in Physics, Springer.

79 Mussot, A., Kudlinski, A., Droques, M., Szriftgiser, P., and Akhmediev, N. (2014) Fermi-Pasta-Ulam recurrence in nonlinear fiber optics: The role of reversible and irreversible losses. *Physical Review X*, **4**, 011 054.

80 Onorato, M., Vozella, L., Proment, D., and Lvov, Y.V. (2015) Route to thermalization in the α-fermi–pasta–ulam system. *Proceedings of the National Academy of Sciences*, **112** (14), 4208–4213.

81 Lake, B., Yuen, H., Rundgaldier, H., and Ferguson, W. (1977) Nonlinear deep-water waves: theory and experiment. part 2. evolution of a continuous wave train. *Journal of Fluid Mechanics*, **83**, 49.

82 Wu, M. and Patton, C. (2007) Experimental observation of Fermi-Pasta-Ulam recurrence in a nonlinear feedback ring system. *Physical Review Letters*, **98**, 047 202.

83 Simaeys, G., Emplit, P., and Haelterman, M. (2001) Experimental demonstration of the Fermi-Pasta-Ulam recurrence in a modulationally unstable optical wave. *Physical Review Letters*, **87**, 033 902.

84 Cambournac, C., Maillotte, H., Lantz, E., Dudley, J.M., and Chauvet, M. (2002) Spatiotemporal behavior of periodic arrays of spatial solitons in a planar waveguide with relaxing Kerr nonlinearity. *Journal of the Optical Society of America B*, **19** (3), 574–585.

85 Hammani, K., Wetzel, B., Kibler, B., *et al.* (2011) Spectral dynamics of modulation instability described using Akhmediev breather theory. *Optics Letters*, **36** (11), 2140–2142.

86 Barviau, B., Garnier, J., Xu, G., *et al.* (2013) Truncated thermalization of incoherent optical waves through supercontinuum generation in photonic crystal fibers. *Physical Review A*, **87** (3), 035 803.

87 Travers, J.C., Rulkov, A.B., Cumberland, B.A., Popov, S.V., and Taylor, J.R. (2008) Visible supercontinuum generation in photonic crystal fibers with a 400w continuous wave fiber laser. *Optics Express*, **16** (19), 14 435–14 447.

88 Michel, C., Garnier, J., Suret, P., Randoux, S., and Picozzi, A. (2011) Kinetic description of random optical waves and anomalous thermalization of a nearly integrable wave system. *Letters In Mathematics and Physics*, **96** (1), 415–447.

89 Ablowitz, M. and Segur, H. (1981) *Solitons and the Inverse Scattering Transform*, SIAM, Society for Industrial and Applied Mathematics, 1981.

90 Ghofraniha, N., Conti, C., Ruocco, G., and Trillo, S. (2007) Shocks in nonlocal media. *Physical Review Letters*, **99**, 043 903.

91 Conti, C., Fratalocchi, A., Peccianti, M., Ruocco, G., and Trillo, S. (2009) Observation of a gradient catastrophe generating solitons. *Physical Review Letters*, **102**, 083 902.

92 Ghofraniha, N., Gentilini, S., Folli, V., DelRe, E., and Conti, C. (2012) Shock waves in disordered media. *Physical Review Letters*, **109**, 243 902.

93 El, G. and Kamchatnov, A. (2005) Kinetic equation for a dense soliton gas. *Physical Review Letters*, **95**, 204 101.

94 Zakharov, V. (2009) Turbulence in integrable systems. *Studies in Applied Mathematics*, **122**, 219.

95 Barviau, B., Randoux, S., and Suret, P. (2006) Spectral broadening of a multimode continuous-wave optical field propagating in the normal dispersion regime of a fiber. *Optics Letters*, **31** (11), 1696–1698.

96 Janssen, P. (2003) Nonlinear four-wave interactions and freak waves. *Journal of Physical Oceanography*, **33**, 864.

97 Annenkov, S.Y. and Shrira, V.I. (2006) Role of non-resonant interactions in the evolution of nonlinear random water wave fields. *Journal of Fluid Mechanics*, **561**, 181–207.

98 Randoux, S., Walczak, P., Onorato, M., and Suret, P. (2014) Intermittency in integrable turbulence. *Physical Review Letters*, **113**, 113 902.

99 Costa, A., Osborne, A.R., Resio, D.T., Alessio, S., Chrivì, E., Saggese, E., Bellomo, K., and Long, C.E. (2014) Soliton turbulence in shallow water ocean surface waves. *Physical Review Letters*, **113**, 108 501.

100 Derevyanko, S.A. and Prilepsky, J.E. (2008) Random input problem for the nonlinear Schrödinger equation. *Physical Review E*, **78**, 046 610.

101 Derevyanko, S.A. (2011) Appearance of bound states in random potentials with applications to soliton theory. *Physical Review E*, **84**, 016 601.

102 Bromberg, Y., Lahini, Y., Small, E., and Silberberg, Y. (2010) Hanbury Brown and Twiss interferometry with interacting photons. *Nature Photonics*, **4**, 721.

103 Derevyanko, S. and Small, E. (2012) Nonlinear propagation of an optical speckle field. *Physical Review A*, **85**, 053 816.

104 Davis, M., Morgan, S., and Burnett, K. (2001) Simulations of Bose fields at finite temperature. *Physical Review Letters*, **87**, 160 402.

105 Connaughton, C., Josserand, C., Picozzi, A., Pomeau, Y., and Rica, S. (2005) Condensation of classical nonlinear waves. *Physical Review Letters*, **95**, 263 901.

106 During, G., Picozzi, A., and Rica, S. (2009) Breakdown of weak-turbulence and nonlinear wave condensation. *Physica D*, **238**, 1524.

107 Aschieri, P., Garnier, J., Michel, C., Doya, V., and Picozzi, A. (2011) Condensation and thermalization of classsical optical waves in a waveguide. *Physical Review A*, **83**, 033 838.

108 Picozzi, A. and Rica, S. (2012) Condensation of classical optical waves beyond the cubic nonlinear Schrödinger equation. *Optics Communications*, **285**, 5440.

109 Conti, C., Leonetti, M., Fratalocchi, A., Angelani, L., and Ruocco, G. (2008) Condensation in disordered lasers: Theory, 3d+1 simulations, and experiments. *Physical Review Letters*, **101**, 143 901.

110 Turitsyna, E., Falkovich, G., Mezentsev, V., and Turitsyn, S. (2009) Optical turbulence and spectral condensate in long-fiber lasers. *Physical Review A*, **80**, 031 804.

111 Weill, R., Fischer, B., and Gat, O. (2010) Light-mode condensation in actively-mode-locked lasers. *Physical Review Letters*, **104** (17), 173 901.

112 Klaers, J., Schmitt, J., Vewinger, F., and Weitz, M. (2010) Bose-Einstein condensation of photons in an optical microcavity. *Nature*, **468**, 545.

113 Michel, C., Haelterman, M., Suret, P., *et al.* (2011) Thermalization and condensation in an incoherently pumped passive optical cavity. *Physical Review A*, **84**, 033 848.

114 Turitsyn, S.K., Babin, S.A., Turitsyna, E.G., *et al.* (2013) *Optical Wave Turbulence*, Eds. V. Shira and S. Nazarenko, *Wave Turbulence*, World Scientific Series on Nonlinear Science Series A: Volume 83.

115 Turitsyna, E., Falkovich, G., El-Taher, A., *et al.* (2012) Optical turbulence and spectral condensate in long fibre lasers. *Proceedings of Royal Society A*, **468**, 2145.

116 Turitsyna, E., Smirnov, S., Sugavanam, S., *et al.* (2013) The laminar-turbulent transition in a fibre laser. *Nature Photonics*, **7** (10), 783–786.

117 Kirton, P. and Keeling, J. (2013) Nonequilibrium model of photon condensation. *Physical Review Letters*, **111**, 100 404.

118 Fischer, B. and Weill, R. (2012) When does single-mode lasing become a condensation phenomenon? *Optics Express*, **20** (24), 26 704–26 713.

119 Carusotto, I. and Ciuti, C. (2013) Quantum fluids of light. *Review of Modern Physics*, **85**, 299–366.

120 Weill, R., Levit, B., Bekker, A., Gat, O., and Fischer, B. (2010) Laser light condensate: experimental demonstration of light-mode condensation in actively mode locked laser. *Optics Express*, **18** (16), 16 520–16 525.

121 Gordon, A. and Fischer, B. (2002) Phase transition theory of many-mode ordering and pulse formation in lasers. *Physical Review Letters*, **89**, 103 901.

122 Weill, R., Rosen, A., Gordon, A., Gat, O., and Fischer, B. (2005) Critical behavior of light in mode-locked lasers. *Physical Review Letters*, **95**, 013 903.

123 Churkin, D.V., Kolokolov, I.V., Podivilov, E.V., *et al.* (2015) Wave kinetics of random fibre lasers. *Nature Communications*, **2**.

124 Babin, S.A., Churkin, D.V., Ismagulov, A.E., Kablukov, S.I., and Podivilov, E.V. (2007) Four-wave-mixing-induced turbulent spectral broadening in a long Raman fiber laser. *Journal of the Optical Society of America B*, **24**, 1729.

125 Dalloz, N., Randoux, S., and Suret, P. (2010) Influence of dispersion of fiber Bragg grating mirrors on formation of optical power spectrum in Raman fiber lasers. *Optics Letters*, **35**, 2505–2507.

126 Randoux, S., Dalloz, N., and Suret, P. (2011) Intracavity changes in the field statistics of Raman fiber lasers. *Optics Letters*, **36** (6), 790–792.

127 Turitsyna, E.G., Turitsyn, S.K., and Mezentsev, V.K. (2010) Numerical investigation of the impact of reflectors on spectral performance of Raman fibre laser. *Optics Express*, **18**, 4469.

128 Turitsyn, S.K., Babin, S.A., El-Taher, A.E., *et al.* (2010) Random distributed feedback fibre laser. *Nature Photonics*, **4**, 231.

129 Turitsyn, S.K., Babin, S.A., Churkin, D.V., *et al.* (2014) Random distributed feedback fibre lasers. *Physics Reports*, **542** (2), 133–193. Random Distributed Feedback Fibre Lasers.

130 L'vov, V.S., L'vov, Y., Newell, A.C., and Zakharov, V. (1997) Statistical description of acoustic turbulence. *Physical Review E*, **56**, 390–405.

131 Leo, F., Coen, S., Kockaert, P., *et al.* (2010) Temporal cavity solitons in one-dimensional Kerr media as bits in an all-optical buffer. *Nature Photonics*, **4**, 471.

132 Arecchi, T., Boccalettic, S., and Ramazza, P. (1999) Pattern formation and competition in nonlinear optics. *Physics Reports*, **318**, 1.

133 Klaers, J., Vewinger, F., and Weitz, M. (2010) Thermalization of a two-dimensional photonic gas in a white wall photon box. *Nature Physics*, **6** (7), 512–515.

134 Conforti, M., Mussot, A., Fatome, J., *et al.* (2015) Turbulent dynamics of an incoherently pumped passive optical fiber cavity: Quasisolitons, dispersive waves, and extreme events. *Physical Review A*, **91**, 023 823.

135 Hammani, K., Kibler, B., Finot, C., and Picozzi, A. (2010) Emergence of rogue waves from optical turbulence. *Physics Letters A*, **374**, 3585.

136 Kibler, B., Hammani, K., Finot, C., and Picozzi, A. (2011) Rogue waves, rational solitons and wave turbulence theory. *Physics Letters A*, **375**, 3149.

137 Xu, G., Garnier, J., Trillo, S., and Picozzi, A. (2013) Spectral dynamics of incoherent waves with a noninstantaneous nonlinear response. *Optics Letters*, **38** (16), 2972–2975.

138 Montes, C. (1979) Photon soliton and fine structure due to nonlinear compton scattering. *Physical Review A*, **20**, 1081.

139 Xu, G., Garnier, J., Conforti, M., and Picozzi, A. (2014) Generalized description of spectral incoherent solitons. *Optics Letters*, **39** (14), 4192–4195.

140 Musher, S., Rubenchik, A., and Zakharov, V. (1976) Weak Langmuir turbulence of an isothermal plasma. *JETP*, **42**, 80.
141 Xu, G., Garnier, J., Trillo, S., and Picozzi, A. (2014) Impact of self-steepening on incoherent dispersive spectral shocks and collapselike spectral singularities. *Physical Review A*, **90**, 013 828.
142 Whitham, G. (1974) *Linear and Nonlinear Waves*, Wiley, New York.
143 Gurevich, A. and Pitaevskii, L. (1974) Nonstationary structure of a collisionless shock wave. *Soviet Physics JETP*, **38**, 291.
144 Taylor, R., Baker, D., and Ikezi, H. (1970) Observation of collisionless electrostatic shocks. *Physical Review Letters*, **24**, 206.
145 Hoefer, M.A., Ablowitz, M.J., Coddington, I., *et al.* (2006) Dispersive and classical shock waves in Bose-Einstein condensates and gas dynamics. *Physical Review A*, **74**, 023 623.
146 Chang, J.J., Engels, P., and Hoefer, M.A. (2008) Formation of dispersive shock waves by merging and splitting Bose-Einstein condensates. *Physical Review Letters*, **101**, 170 404.
147 Wan, W., Jia, S., and Fleischer, J. (2007) Dispersive, superfluid-like shock waves in nonlinear optics. *Nature Physics*, **3**, 46.
148 Ghofraniha, N., Amato, L.S., Folli, V., *et al.* (2012) Measurement of scaling laws for shock waves in thermal nonlocal media. *Optics Letters*, **37** (12), 2325–2327.
149 Conforti, M., Baronio, F., and Trillo, S. (2013) Competing wave-breaking mechanisms in quadratic media. *Optics Letters*, **38** (10), 1648–1650.
150 Wiegmann, P. (2012) Nonlinear hydrodynamics and fractionally quantized solitons at the fractional quantum hall edge. *Physical Review Letters*, **108**, 206 810.
151 Mo, Y.C., Kishek, R.A., Feldman, D., *et al.* (2013) Experimental observations of soliton wave trains in electron beams. *Physical Review Letters*, **110**, 084 802.
152 Fratalocchi, A., Armaroli, A., and Trillo, S. (2011) Time-reversal focusing of an expanding soliton gas in disordered replicas. *Physical Review A*, **83**, 053 846.
153 Gentilini, S., Ghofraniha, N., DelRe, E., and Conti, C. (2013) Shock waves in thermal lensing. *Physical Review A*, **87**, 053 811.
154 Constantin, P., Lax, P., and Majda, A. (1985) A simple one-dimensional model for the three-dimensional vorticity equation. *Communications on Pure and Applied Mathematics*, **38**, 715–724.
155 Fokas, A. and Ablowitz, M. (1983) The inverse scattering transform for the Benjamin-ono equation – a pivot to multidimensional problems. *Studies in Applied Mathematics*, **68**, 1.
156 Michel, C., Kibler, B., Garnier, J., and Picozzi, A. (2012) Temporal incoherent solitons supported by a defocusing nonlinearity with anomalous dispersion. *Physical Review A*, **86** (4), 041 801.
157 Saleh, M.F., Chang, W., Travers, J.C., Russell, P.S.J., and Biancalana, F. (2012) Plasma-induced asymmetric self-phase modulation and modulational instability in gas-filled hollow-core photonic crystal fibers. *Physical Review Letters*, **109**, 113 902.
158 Sauter, A., Pitois, S., Millot, G., and Picozzi, A. (2005) Incoherent modulation instability in instantaneous nonlinear Kerr media. *Optics Letters*, **30**, 2143–2145.
159 Skryabin, D., Luan, F., Knight, J., and Russell, P. (2003) Soliton self-frequency shift cancellation in photonic crystal fibers. *Science*, **301**, 1705.

160 Xu, G., Garnier, J., and Picozzi, A. (2014) Spectral long-range interaction of temporal incoherent solitons. *Optics Letters*, **39** (3), 590–593.

161 Onorato, M., Osborne, A., Serio, M., *et al.* (2006) Extreme waves, modulational instability and second order theory: wave flume experiments on irregular waves. *European Journal of Mechanics-B/Fluids*, **25** (5), 586–601.

162 Akhmediev, N., Soto-Crespo, J., and Ankiewicz, A. (2009) Extreme waves that appear from nowhere: On the nature of rogue waves. *Physics Letters A*, **373** (25), 2137–2145.

163 Ankiewicz, A., Soto-Crespo, J., and Akhmediev, N. (2010) Rogue waves and rational solutions of the Hirota equation. *Physical Review E*, **81** (4), 046 602.

164 Viotti, C., Dutykh, D., Dudley, J.M., and Dias, F. (2013) Emergence of coherent wave groups in deep-water random sea. *Physical Review E*, **87**, 063 001.

165 Sugny, D., Picozzi, A., Lagrange, S., and Jauslin, H. (2009) Role of singular tori in the dynamics of spatiotemporal nonlinear wave systems. *Physical Review Letters*, **103**, 034 102.

166 Conti, C., Schmidt, M.A., Russell, P.S.J., and Biancalana, F. (2010) Highly noninstantaneous solitons in liquid-core photonic crystal fibers. *Physical Review Letters*, **105**, 263 902.

167 Saleh, M.F., Chang, W., Hölzer, P., *et al.* (2011) Theory of photoionization-induced blueshift of ultrashort solitons in gas-filled hollow-core photonic crystal fibers. *Physical Review Letters*, **107** (20), 203 902.

168 Marini, A., Conforti, M., Della Valle, *et al.* (2013) Ultrafast nonlinear dynamics of surface plasmon polaritons in gold nanowires due to the intrinsic nonlinearity of metals. *New Journal of Physics*, **15** (1), 013 033.